https://ntrs.nasa.gov/search.jsp?R=20140003390 2019-08-29T14:48:07+00:00Z

NASA/TP–2013-218051

Aeroservoelastic Testing of Free Flying Wind Tunnel Models

Part 1: A Sidewall Supported Semispan Model Tested for Gust Load Alleviation and Flutter Suppression

Robert C. Scott
Langley Research Center, Hampton, Virginia

Travis K. Vetter
Northrop Grumman Corporation, El Segundo, California

Kevin B. Penning
Lockheed Martin, Fort Worth, Texas

David A. Coulson
Analytical Services and Materials, Inc., Hampton, Virginia

Jennifer Heeg
Langley Research Center, Hampton, Virginia

October 2013

NASA STI Program . . . in Profile

Since its founding, NASA has been dedicated to the advancement of aeronautics and space science. The NASA scientific and technical information (STI) program plays a key part in helping NASA maintain this important role.

The NASA STI program operates under the auspices of the Agency Chief Information Officer. It collects, organizes, provides for archiving, and disseminates NASA's STI. The NASA STI program provides access to the NASA Aeronautics and Space Database and its public interface, the NASA Technical Report Server, thus providing one of the largest collections of aeronautical and space science STI in the world. Results are published in both non-NASA channels and by NASA in the NASA STI Report Series, which includes the following report types:

- TECHNICAL PUBLICATION. Reports of completed research or a major significant phase of research that present the results of NASA Programs and include extensive data or theoretical analysis. Includes compilations of significant scientific and technical data and information deemed to be of continuing reference value. NASA counterpart of peer-reviewed formal professional papers, but having less stringent limitations on manuscript length and extent of graphic presentations.

- TECHNICAL MEMORANDUM. Scientific and technical findings that are preliminary or of specialized interest, e.g., quick release reports, working papers, and bibliographies that contain minimal annotation. Does not contain extensive analysis.

- CONTRACTOR REPORT. Scientific and technical findings by NASA-sponsored contractors and grantees.

- CONFERENCE PUBLICATION. Collected papers from scientific and technical conferences, symposia, seminars, or other meetings sponsored or co-sponsored by NASA.

- SPECIAL PUBLICATION. Scientific, technical, or historical information from NASA programs, projects, and missions, often concerned with subjects having substantial public interest.

- TECHNICAL TRANSLATION. English-language translations of foreign scientific and technical material pertinent to NASA's mission.

Specialized services also include organizing and publishing research results, distributing specialized research announcements and feeds, providing information desk and personal search support, and enabling data exchange services.

For more information about the NASA STI program, see the following:

- Access the NASA STI program home page at *http://www.sti.nasa.gov*

- E-mail your question to help@sti.nasa.gov

- Fax your question to the NASA STI Information Desk at 443-757-5803

- Phone the NASA STI Information Desk at 443-757-5802

- Write to:
  STI Information Desk
  NASA Center for AeroSpace Information
  7115 Standard Drive
  Hanover, MD 21076-1320

NASA/TP–2013-218051

Aeroservoelastic Testing of Free Flying Wind Tunnel Models

Part 1: A Sidewall Supported Semispan Model Tested for Gust Load Alleviation and Flutter Suppression

Robert C. Scott
Langley Research Center, Hampton, Virginia

Travis K. Vetter
Northrop Grumman Corporation, El Segundo, California

Kevin B. Penning
Lockheed Martin, Fort Worth, Texas

David A. Coulson
Analytical Services and Materials, Inc., Hampton, Virginia

Jennifer Heeg
Langley Research Center, Hampton, Virginia

National Aeronautics and
Space Administration

Langley Research Center
Hampton, Virginia 23681-2199

October 2013

The use of trademarks or names of manufacturers in this report is for accurate reporting and does not constitute an official endorsement, either expressed or implied, of such products or manufacturers by the National Aeronautics and Space Administration.

Available from:

NASA Center for AeroSpace Information
7115 Standard Drive
Hanover, MD 21076-1320
443-757-5802

Abstract

This is part 1 of a two part document. Part 2 is titled: "Aeroservoelastic Testing of Free Flying Wind Tunnel Models Part 2: A Centerline Supported Fullspan Model Tested for Gust Load Alleviation." A team comprised of the Air Force Research Laboratory (AFRL), Northrop Grumman, Lockheed Martin, and the NASA Langley Research Center conducted three aeroservoelastic wind tunnel tests in the Transonic Dynamics Tunnel to demonstrate active control technologies relevant to large, flexible vehicles. In the first of these three tests, a semispan, aeroelastically scaled, wind tunnel model of a flying wing SensorCraft vehicle was mounted to a force balance to demonstrate gust load alleviation. In the second and third tests, the same wing was mated to a new, multi-degree of freedom, sidewall mount. This mount allowed the half-span model to translate vertically and pitch at the wing root, allowing better simulation of the full span vehicle's rigid body modes. Gust load alleviation (GLA) and Body freedom flutter (BFF) suppression were successfully demonstrated. The rigid body degrees-of-freedom required that the model be flown in the wind tunnel using an active control system. This risky mode of testing necessitated that a model arrestment system be integrated into the new mount. The safe and successful completion of these free flying tests required the development and integration of custom hardware and software. This paper describes the many systems, software, and procedures that were developed as part of this effort.

Contents

1 Introduction **6**

2 Transonic Dynamics Tunnel **8**

3 Wing and Mount System **9**
- 3.1 Wing . . . 10
- 3.2 Mount System . . . 14
- 3.3 Test Configurations . . . 15

4 Signal Routing, Processing, and Control **16**
- 4.1 DCS Hardware and Development Environment . . . 17
- 4.2 Hydraulics and Snubber Control System . . . 18

5 WatchDog System **18**
- 5.1 Emergency Controller . . . 20
- 5.2 WatchDog Snub Logic . . . 21
- 5.3 NG—Combined Parameters . . . 21
- 5.4 LM—Combined Parameters . . . 22

6 Flight Control Schemes **22**
- 6.1 Takeoff Launch Scheme . . . 22
- 6.2 Release Launch Scheme . . . 24

7 Testing Procedures **27**
- 7.1 Open-Loop Flutter Clearance . . . 29
- 7.2 Snubbed Flight Clearance and Emergency Controller Validation . . . 29
- 7.3 Gust Load Alleviation Testing . . . 30
- 7.4 Reduced Static Margin Testing . . . 32
- 7.5 BFF Suppression Testing . . . 32

8 Concluding Remarks **33**

9 Acknowledgements **34**

A Flap Actuator Response **37**

B Snubbing System Performance **38**

C Rail Friction and Lift Augmentation System (LAS) **40**

D Development of LM Combined Parameters **42**

List of Tables

1 Model boundary conditions, mount system states, and 1st bending mode frequency. . . . 15

D1 WatchDog system performance assessed using five hard landing cases from Test 593. . . . 44

List of Figures

1 NASA Langley TDT tests for the HiLDA and AEI programs. 6
2 Illustration of AEI apparatus installed in TDT during Test 598. 7
3 NASA Langley TDT. 9
4 Illustration of the TDT Air Stream Oscillating System (AOS). 10
5 Original, 3 DOF mount configuration used in Test 593. 11
6 Revised, 2 DOF mount configuration used in Test 598. 12
7 Photo of the HiLDA model taken from TDT settling chamber. 13
8 Wing instrumentation used for the AEI TDT tests (593 and 598). String potentiometers used for measuring pitch angle (Θ), vertical position (PZ), vertical rate (VZ), and moving mass position are not shown. 13
9 Signal routing used in Tests 593 and 598. 16
10 dSpace and snubber control block diagram. 17
11 Snub control chassis containing the snub control system with manual Snub! switch and hydraulic pressure displays. 19
12 Worst case overload condition from Test 593, point 1833. The bending moment is measured from strain gauge SBI1 shown in figure 8 corrected for outboard wing weight. 20
13 WatchDog system snub logic block diagram. 20
14 Control law and FlightMode logic developed by Northrop Grumman. 22
15 Data acquired while using TakeOff launch scheme to achieve trimmed flight. Test 598, points 1274, 1275, and 1276. 23
16 Trim and suppression control loops along with FlightMode logic developed by Lockheed Martin. 25
17 Data acquired while using Release launch scheme to achieve trimmed flight. Test 598, point 2384. 26
18 Portion of the TDT heavy gas operating envelope showing data acquired during Test 598 where red represents the heavy weight configuration and green represents the light weight configuration. 28
19 Time traces of vertical position, pitch angle, and bending moment while AOS transitioning from 0.7 to 0.5 Hz. WatchDog Snub! engagement shown along with subsequent vertical position ramp down. Test 598, point 4891. The bending moment was measured from strain gauge SBI1 (figure 8) corrected for outboard wing weight. 31
20 Time traces of vertical position, pitch angle, and bending moment while AOS sweeping from 9.5 to 2.0 to 9.5 Hz. Test 598, point 3182. The bending moment is measured from strain gauge SBI1 (figure 8) corrected for outboard wing weight. 32
21 Body freedom flutter time traces for trim only control, light model. WatchDog Snub! engagement shown along with subsequent vertical position ramp down. Test 598, point 3525. The bending moment is measured from strain gauge SBI1 (figure 8) corrected for outboard wing weight. 33
A1 Flap transfer function estimates for beginning (solid), middle (dash), and end (dot dash) of Test 598, points 216, 1600, and 5409. 38
B1 Snubber system time delay experiments, hydraulics at 2000 psi. 39
C1 LAS and wing mounted load cell moving average data acquired during wing vertical translation. Test 598, points 212 (blue) and 3237 (green). 41
C2 LAS load cell data acquired during three different launch and flight sequences. Test 598, points 3245, 3435, and 3455. (Forward load cell data is blue and the aft load cell data is green). 41
D1 Lockheed Martin combined parameter block diagram. 42

D2 Hard landing case plot of vertical position, pitch angle, TE2 command, and wing root bending moment with Snub! command indicated. Test 593, point 1252. The bending moment is measured from strain gauge SBI1 shown in figure 8 corrected for outboard wing weight. 43
D3 Hard landing case comparing nominal WatchDog Snub! command with the Snub! command generated by the LM combined parameters where two values of assumed time delay were used in the feed forward estimator. Test 593, point 1252. 44

Nomenclature

AEI	Aerodynamic Efficiency Improvement
AFRL	Air Force Research Laboratory
AOS	airstream oscillating system
ASE	aeroservoelasticity
BFF	body freedom flutter
CG	center of gravity
DAS	Data Acquisition System
DCS	Digital Control System
DOF	degree of freedom
dSpace1	DCS for Servo PID loops and WatchDog
dSpace2	DCS for trim, GLA, & BFF suppression
δ_o	emergency controller command bias
FS	flutter suppression
GLA	gust load alleviation
GUI	Graphical User Interface
HiLDA	High Lift over Drag Active Wing
LAS	lift augmentation system
LE	leading edge flap
LM	Lockheed Martin
LQG	Linear Quadratic Gaussian
NG	Northrop Grumman
PID	proportional integral derivative
PZ	vertical position (PZ = 0 at centerline), in
RVDT	rotary variable differential transducer
Snub!	command to engage snubbing system
T	time, s
TE	trailing edge flap 1, 2, 3, or 4
TDT	Transonic Dynamics Tunnel
Θ	pitch displacement, deg
$\dot{\Theta}$	pitch rate, deg/s
V	Volts
VZ	vertical velocity, in/s
WatchDog	software for triggering Snub! command
WD	abbreviation for WatchDog
WoW	weight on wheels

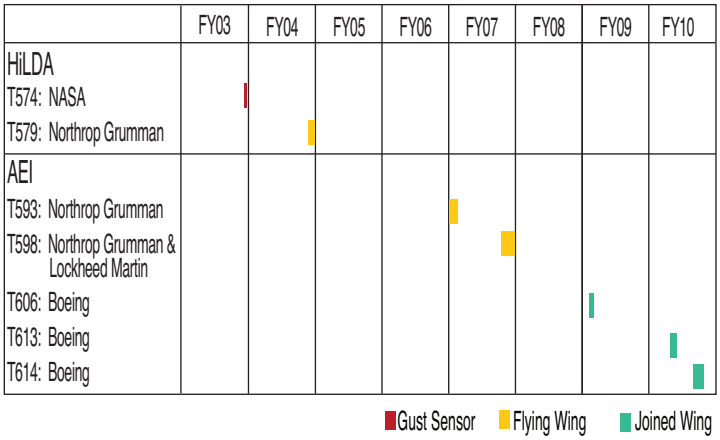

Figure 1. NASA Langley TDT tests for the HiLDA and AEI programs.

1 Introduction

In the Fall of 2007, the Air Force Research Laboratory (AFRL), Northrop Grumman (NG), Lockheed Martin (LM), and the NASA Langley Research Center, successfully completed the third of a series of three wind tunnel tests of an aeroelastically scaled wind tunnel model of a flying wing SensorCraft vehicle concept. The AFRL SensorCraft is a technology portfolio of advanced sensors, communications links, air vehicle components and propulsion elements. AFRL is pursuing these technology developments for future high-altitude, long-endurance, unmanned surveillance platforms [1]. Two research programs intended to develop technologies relevant to these large, flexible vehicles are the High Lift over Drag Active (HiLDA) Wing and the Aerodynamic Efficiency Improvement (AEI) programs [2]. The goals of the HiLDA and AEI wind tunnel tests included the demonstration of gust load alleviation (GLA), an enabling technology for a SensorCraft vehicle that will allow it to have reduced structural weight thereby increasing endurance, range, and payload capacity.

The HiLDA and AEI wind tunnel investigations were conducted in the NASA Langley Transonic Dynamics Tunnel (TDT). Three flying wing wind tunnel tests and five joined-wing [3, 4] wind tunnel tests are depicted in figure 1. The first two wind tunnel tests were conducted as part of the HiLDA program. The first was a short test of several candidate sensors for measuring gust flow angle. The HiLDA flying wing was tested September 2004 with GLA being demonstrated on a cantilevered mount using the model's five active control surfaces [5–7]. This paper will focus on the flying wing tests conducted as part of the AEI program, while the the joined wing tests will be covered in a separate report.

The HiLDA wing was retested in October 2006 as part of the AEI program, where it was mated to a new, multi-degree of freedom (DOF) mount. This mount allowed the half span model to translate vertically and pitch at the wing root, allowing better simulation of the full span vehicle's rigid body modes. Following some modifications to the mount system, the wing was tested on the mount again in the summer of 2007. Figure 2 depicts the wing and mount system in the final configuration used in Test 598. The upstream flow angle sensor or gust sniffer is also shown in the image. During this test, GLA control systems were demonstrated in the presence of gusts generated by the TDT airstream oscillating system (AOS) with peak wing bending loads being reduced by up to 60 percent, and body freedom flutter (BFF) suppression control laws were demonstrated with flutter onset dynamic pressure being increased up to 50 percent.

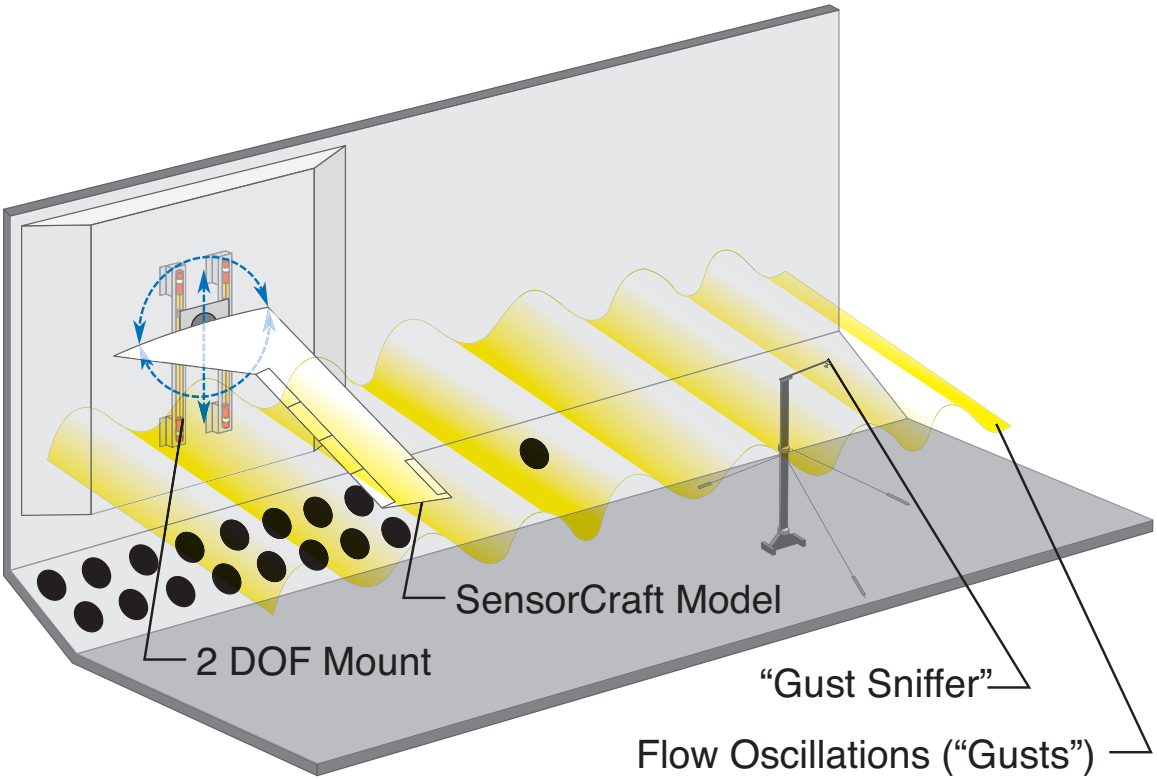

Figure 2. Illustration of AEI apparatus installed in TDT during Test 598.

The large size of the flying wing model along with the rigid body DOF afforded by the new mount system, created many unique challenges to successfully and safely meeting the AEI test objectives. A remotely actuated snubbing system that returned the model to a fixed pitch angle was included in the mount design. Determining how to effectively use this system was critical to the success of the test. Two digital control systems were used: one to implement the actuator servo control loops and the other to implement the trim, GLA, and BFF suppression control loops. For model safety, a snubbing system was integrated with mount system, and the digital control systems included a safety monitoring (WatchDog) system for automatically triggering the snubbing system. The WatchDog system was implemented on the same digital control computer as the servo control loops. Along with these systems, a variety of procedures had to be developed including those for model launch and recovery.

This paper will provide an overview of the AEI flying wing wind tunnel tests from an operational point of view with the focus on systems, procedures, and lessons learned. The paper includes descriptions of the hardware including the wind tunnel, the wing model, the mount system, and other supporting systems developed for this program. The software developed for the digital control systems will be described including the control law architectures and the WatchDog system. The main part of the paper will conclude with a description of the wind tunnel testing procedures that were used. An appendix provides some additional analysis and testing details not covered in the main part of the paper. Throughout the paper, wind tunnel data will be shown where applicable or necessary with an emphasis on the final test of the flying wing, Test 598.

For the purpose of clarity, a brief overview of the model launch schemes, the flight control architectures, and the WatchDog system is warranted. Two model launch schemes were used, the TakeOff and the Release launch schemes developed for use by Northrop Grumman and Lockheed Martin, respectively. Throughout this paper, the TakeOff launch scheme will be associated with the NG control architecture where trim and suppression controllers are combined into a single control loop. The Release launch scheme will be associated with the LM control architecture where trim and suppression controllers are in separate control loops. In addition, a separate set of WatchDog monitored parameters and associated limits are used with each launch scheme. These topics will be discussed separately in the paper.

2 Transonic Dynamics Tunnel

The Langley TDT, depicted in figure 3, is a unique national facility dedicated to identifying, understanding, and solving relevant aeroelastic and aeroservoelastic problems. The TDT is a closed circuit, continuous flow, variable pressure, wind tunnel with a 16 ft square test section with cropped corners [8]. The tunnel uses either air or a heavy gas as the test medium and can operate at total pressures from near vacuum to atmospheric. It has a Mach number range from near zero to 1.2 and is capable of maximum Reynolds numbers of about 3 million per foot in air and 10 million per foot in heavy gas. Until 1996, the TDT used dichlorodifluoromethane (R-12) as the heavy gas test medium; since then the TDT has used 1,1,1,2 tetrafluoroethane(R-134a) [9, 10], an environmentally acceptable alternative to R-12.

The TDT is specially configured for flutter testing, with excellent model visibility from the control room and a rapid tunnel shutdown capability for model safety. Testing in heavy gas has important advantages over testing in air: improved model to full scale similitude (which results in heavier, easier to build models with lower elastic mode frequencies), higher Reynolds numbers, and reduced tunnel power requirements.

Due to the need to perform GLA testing as part of the AEI program, the TDT AOS was used frequently. Figure 4 shows the key features of the AOS system including the biplane

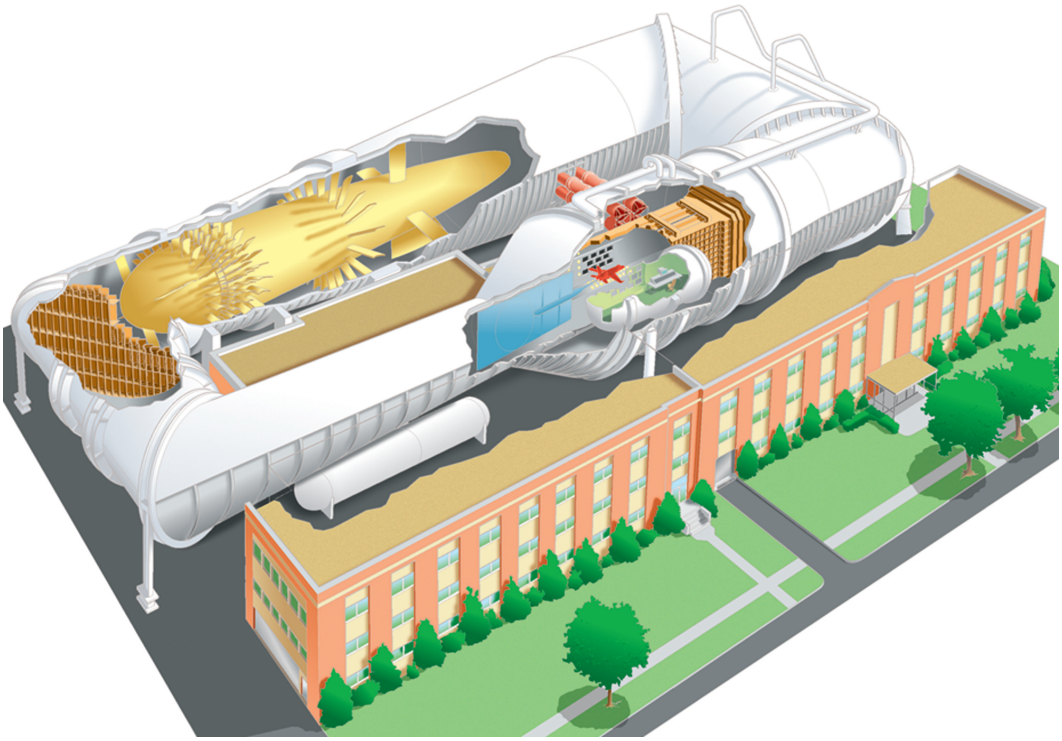

Figure 3. NASA Langley TDT.

arrangement of vanes on either side of the entrance to the test section. Each pair of vanes is driven by a separate hydraulic motor and a flywheel to hold constant vane frequency. While the two pairs of vanes can be run out of phase, this was not done in the AEI test. Vane frequency was adjusted from the TDT control room manually or by using a LabVIEW® system. The amplitude of the vanes is manually adjustable from 0° to 12° peak-to-peak. For most of Test 598, the 12° peak-to-peak setting was used providing approximately ±1° variation in the model angle of attack. For the last week of Test 598, the vane amplitude was reduced to 4° peak-to-peak.

3 Wing and Mount System

The wing and mount system were designed and fabricated by NextGen Aeronautics in Torrance, California. NextGen Aeronautics was a subcontractor to the Northrop Grumman Corporation for the initial development of the wing for Test 579, and later, for the wing modifications and mount system design and fabrication for Test 593. NextGen Aeronautics was a subcontractor to the Lockheed Martin Company for the wing and mount modifications that preceded Test 598. This section of the paper will provide a description of the wing and mount system along with a discussion of the modifications that took place over the life of the program. References 5 and 6 offer a more detailed description of the HiLDA wing, and references 11 and 12 contain details associated with the wing and mount system.

Figure 5 shows the wing and mount system configuration used in Test 593, and figure 6 shows the configuration used in Test 598. These figures should be referred to when reading the sections that follow.

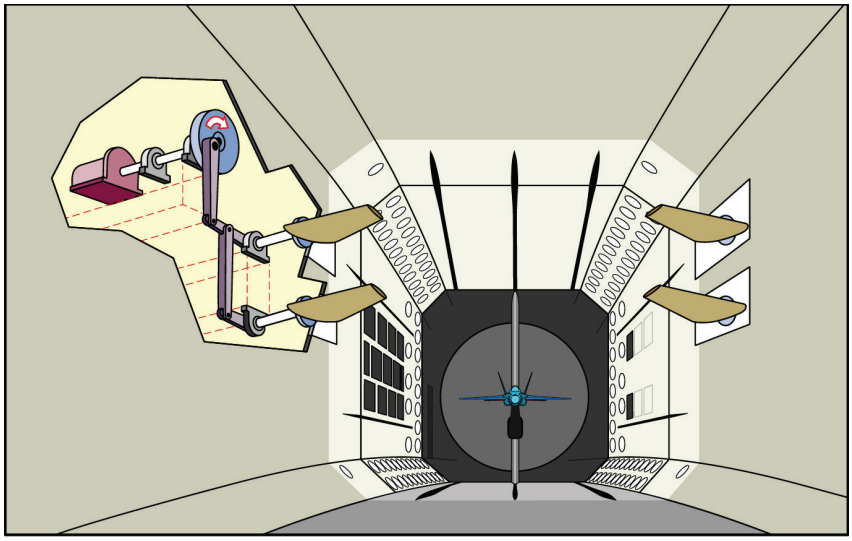

Figure 4. Illustration of the TDT Air Stream Oscillating System (AOS).

3.1 Wing

The wing is a 12 percent length scale, semispan model of a SensorCraft design concept originally designed for use in the HiLDA program. The outboard part of the wing is a spar-pod design where the scaled stiffnesses (EI and GJ distributions) are designed into the flanged aluminum spar, and the aerodynamic shape is provided by discrete fairings, or pods, mounted to the spar. The original set of pods was made from glass-filled nylon-12 (Duraform GF) manufactured using a stereolithography system. The inboard wing was intended to act as a rigid member and consisted of aluminum spars and internal ribs with fiberglass upper and lower skins. The closeout ribs for the inboard wing were stainless steel to provide the structural attachments for the 5 DOF balance at the root and for the outboard, flexible spar at the wing break. Lead weights could be attached to the spar to simulate fuel weight at the take off configuration.

The wing has four evenly spaced trailing edge control surfaces and one leading edge control surface on the outboard, flexible portion of the wing. The five control surfaces were driven by vane-type hydraulic actuators with position measured by rotary variable differential transducers (RVDTs). Two separate hydraulic systems were included in the model so that the trailing edge flaps could be operated at 1,000 psi, while the more heavily loaded leading edge flap could be operated at up to 2,000 psi. Other instrumentation included strain gauges, accelerometers, a pitch-rate gyro, and a gust vane placed in front of the model to allow lead gust information to be fed into the controller. Figure 7 shows a photo of the HiLDA wing installed in the TDT from the settling chamber.

In preparation for the first AEI test, TDT Test 593, several modifications were made to the HiLDA wing. As a result of the new model mount system with additional DOF, overall mass and center of gravity (CG) became important considerations. To adjust the model CG, the LE caps of the inboard part of the wing were modified so that six blocks of lead could be installed to provide up to 30 lb of forward ballast. In addition, a moving mass system was included in the rigid root section that provided remote adjustment of the model CG. The device consisted of a compact stepper motor coupled to a ball screw actuator driving a 32 lb ballast weight. The ballast assembly was restrained by two linear slides with a string potentiometer for position measurement.

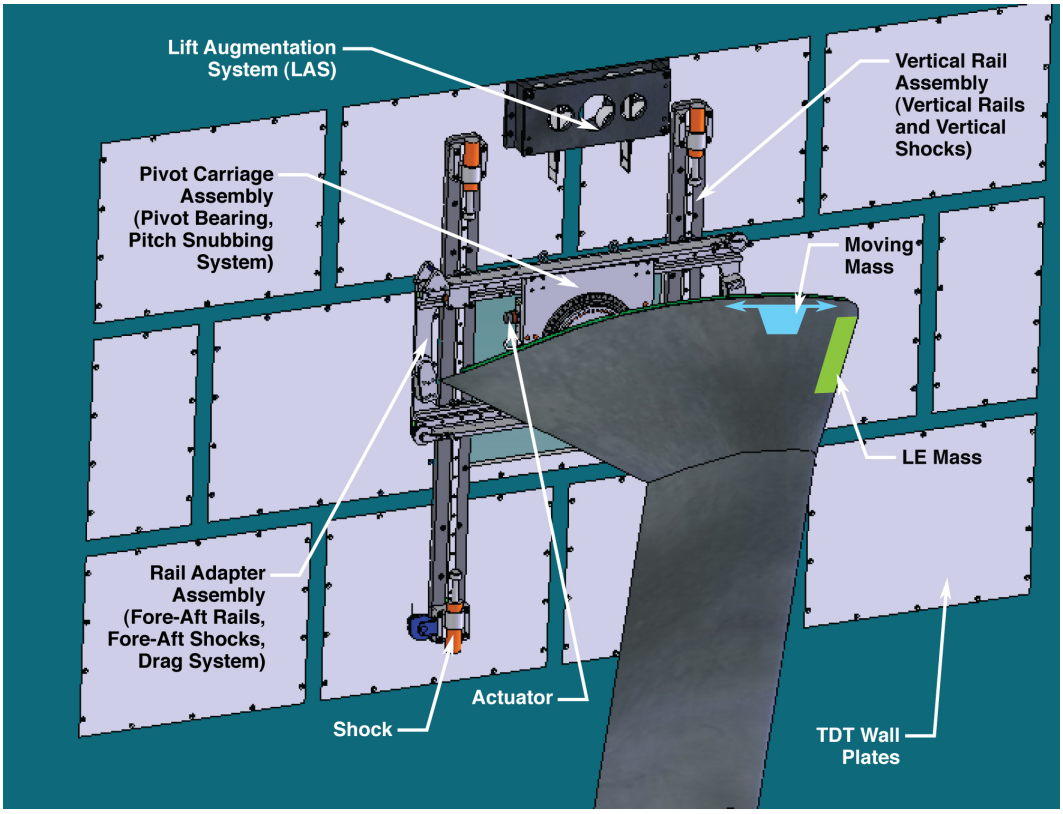

(a) Mount system components.

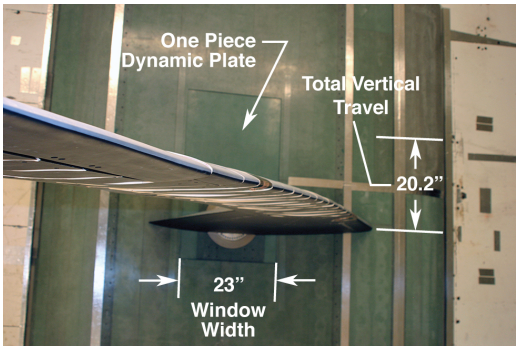

(b) Original fairing assembly with large dynamic plate. Total vertical travel includes 14.2 in of free travel plus the 3 in strokes of the upper and lower shocks.

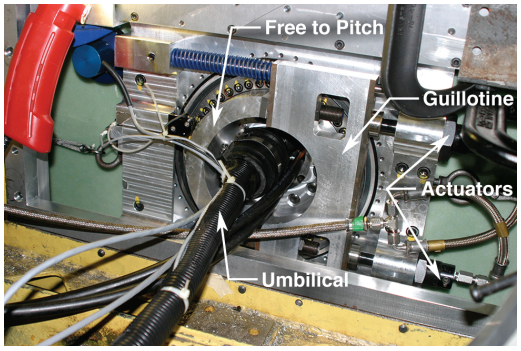

(c) Back side of pivot carriage showing snubbing mechanism and umbilical.

Figure 5. Original, 3 DOF mount configuration used in Test 593.

Modifications to the HiLDA wing's instrumentation suite included changes to the accelerometer locations to better measure the free-free mode shapes and the addition of a pitch rate gyro near the wing root. Figure 8 shows the instrumentation layout used in both AEI tests. Leading edge stagnation point sensor arrays developed by Tao Systems are not depicted in this figure, but they are described in reference 13. To simplify the model's hydraulic requirements, a larger leading edge actuator was built for this test so that it could operate at the same hydraulic pressure as the trailing edge flaps.

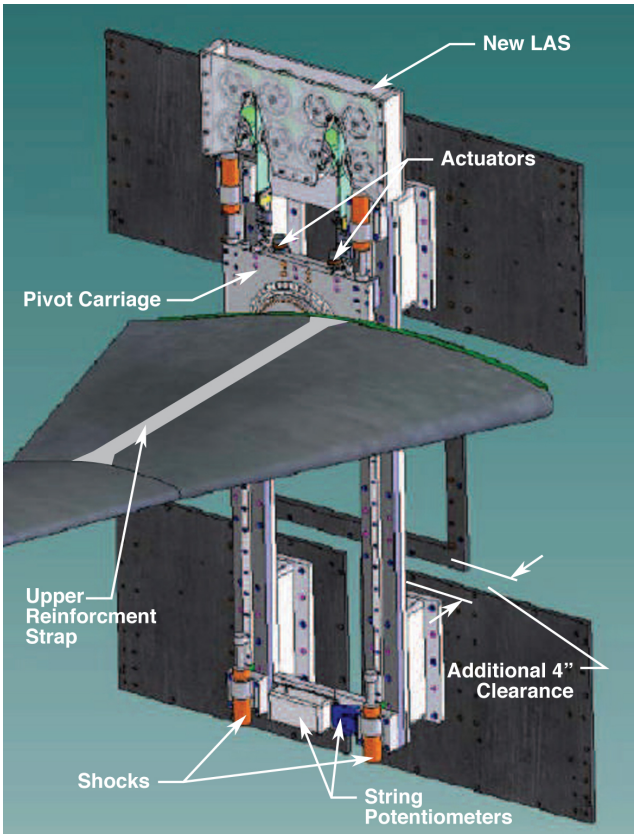

(a) Revised mount system.

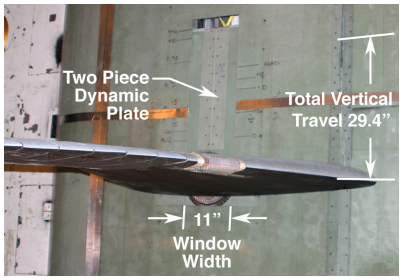

(b) Revised fairing assembly with smaller window and dynamic plate. Total vertical travel includes 23.4 in of free travel plus the 3 in strokes of the upper and lower shocks.

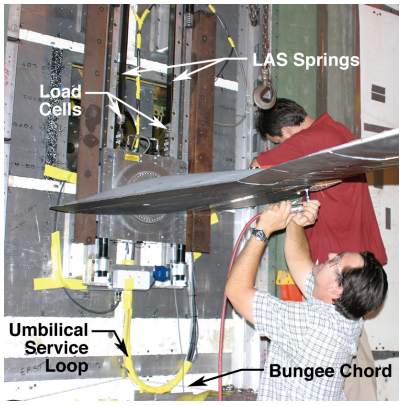

(c) Installed mount system showing umbilical service loop.

Figure 6. Revised, 2 DOF mount configuration used in Test 598.

The pods and control surfaces were redesigned to simplify installation and removal, and they were fabricated using a different material (Watershed 11120) to avoid concerns over moisture absorption. Unfortunately, the 11120 material has a low glass transition temperature, and the pods warped due to elevated temperatures in transit to the TDT.

Changes to the wing in preparation for TDT Test 598 were limited largely to maintenance items; however, two important modifications were made. First, the pod material was changed back to Duraform to avoid heat related warping. Duraform GF was used for the new pods, and Duraform AF was used for the new control surfaces. To minimize moisture absorption, all pod surfaces were sealed using primer. The second modification was deemed necessary when, during inspection, it was determined that the inboard wing had been overloaded during Test 593. Wind tunnel data from this event will be shown later in the paper. A steel strap was added to the upper and lower surfaces of the inboard wing to strengthen the center spar by providing an additional load path between the two stainless steel ribs (figure 6).

Appendix A describes the performance and challenges associated with using and maintaining the wing flap actuators during Test 598.

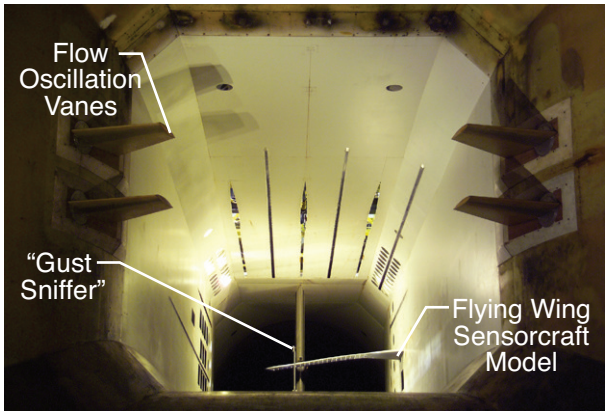

Figure 7. Photo of the HiLDA model taken from TDT settling chamber.

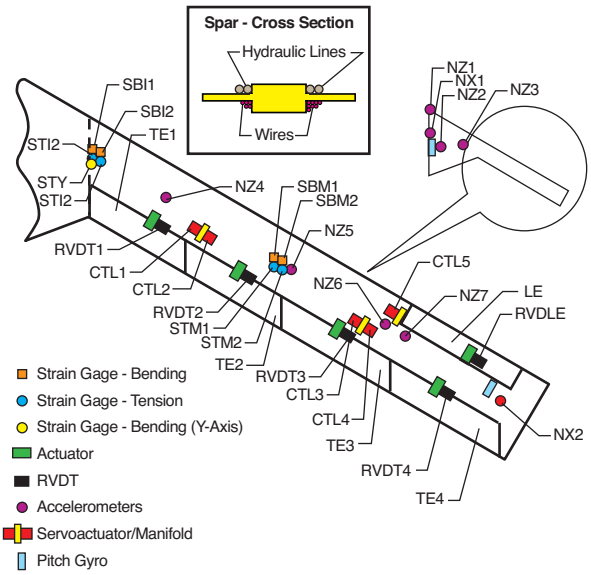

Figure 8. Wing instrumentation used for the AEI TDT tests (593 and 598). String potentiometers used for measuring pitch angle (Θ), vertical position (PZ), vertical rate (VZ), and moving mass position are not shown.

3.2 Mount System

The sidewall multi-DOF mount system evolved considerably over the course of the two TDT tests in which it was used. Initially for Test 593, the mount was configured to provide 3 DOF; pitch, plunge, and fore-aft translation (figure 5). Based on the operational experience gained in Test 593, several significant changes were made to the mount system in preparation for Test 598. These changes included the removal of the fore-aft DOF and a complete redesign of the lift augmentation system. Figure 6 shows the revised system. The key elements of the mount system along with the various design changes will be described next.

The pivot carriage assembly was the heart of the mount system. It consisted of the pivot bearing and the hydraulic pitch snubbing mechanism. The snubber consisted of two linear hydraulic actuators that moved a sliding plate (guillotine) that clamped against alternate ends of the half-circle, free-to-pitch structure that attaches to the wing. Figure 5 depicts the back side of the pivot carriage assembly showing the pitch snub components and the hydraulic/instrumentation umbilical exiting the model through the center of the bearing assembly. A string potentiometer was used to measure model pitch angle during both tests, and another string potentiometer was added prior to Test 598 to provide a direct measurement of the guillotine position. For the unsnubbed condition, the total rotation was controlled by setting the retraction distance of the guillotine by adjusting the hydraulic cylinder mount position. For the snubbed condition, replaceable pads on the free-to-move structure allowed control of the clamped pitch angle. Test 593 had a range of motion of $-12°$ to $+16°$ with a clamped angle of $2°$, and test 598 had a $-6°$ to $8°$ range of motion with a clamped angle of $1°$. The range of motion was restricted to reduce the risk of damaging the model. Appendix B describes experiments used to assess and improve the performance of the snubbing system.

The rail adaptor and vertical rail assemblies provided the translational DOFs via THK 20 mm width rails and guide blocks with vertical and fore-aft position measured using string potentiometers. To minimize impact loads, the vertical rail assembly included dashpot shock absorbers at the top and bottom. During Test 593, Mil-Spec bungee cords, cables, and pulleys were used to restrain the fore-aft DOF. It was determined that the fore-aft DOF was heavily damped, and as a result, no significant fore-aft motion was noted during testing. In preparation for Test 598, the assembly that provided the fore-aft DOF, the rail adaptor, was removed. The pivot carriage assembly was rotated $90°$ and attached directly to the vertical rails (figure 6).

A fairing assembly enclosed the mount system. The fairing consisted of fixed exterior fiberglass panels with a cutout or window that allowed for a range of travel of the wing attachment. The window was covered with a dynamic plate that attached directly to and moved with the pivot carriage assembly. Figure 5 shows the fairing assembly used in Test 593. The elimination of the fore-aft DOF for Test 598 allowed the width of the window to be reduced from 23 in to 11 in (figure 6). As a result, the fixed fairing could be better supported, eliminating contacts between the fixed fairing and the wing root and the fixed fairing and dynamic plate. A smaller, two-piece dynamic plate was used in Test 598. The two-piece design allowed the dynamic plate to be removed for access to the mount system components without removing the wing.

A lift augmentation system (LAS) was required to compensate for the mass of the carriage system and excess inboard wing weight. The first iteration of the LAS consisted of eight constant force springs that provided approximately 40 lb of force each for a total lift augmentation of 320 lb. The springs could be attached to the rail adaptor in groups of two via a lanyard and cable assembly. This first system suffered from high friction associated with the spring tapes twisting and rubbing against the spool frame assembly. The redesigned system used in Test 598 again used eight constant force springs, but because of the weight savings associated with the elimination of the fore-aft DOF and the removal

of the rail adaptor assembly, springs providing 20 lb of force each could be used. These springs attached to the pivot carriage assembly via pinned ball joints with load cells in series so that the LAS force could be monitored during the test. Other design improvements included spring spool assemblies with an improved set of bearings and a LAS frame design that minimized potential spring tape contact points.

The original vertical rail assembly consisted of two independent components that bolted directly to the TDT wall plates as shown in figure 5. As a result of irregularities in the test section wall, shimming was necessary to avoid binding the plunge DOF. Also, the hydraulic/instrumentation umbilical had to exit straight out of the assembly as shown in figure 5. Because there was limited space between the pivot carriage assembly and the test section wall, free vertical travel was restricted to ± 7.1 in of the designed ± 12 in to avoid cutting the umbilical on the opening in the test section wall. The free travel does not include the 3 in strokes of the upper and lower shocks, so total vertical travel is 6 in greater than the free travel. The redesigned mount shown in figure 6 included a new standoff support frame that simplified mount installation and provided an additional 4 in of clearance from the wind tunnel wall. These changes allowed the hydraulic/instrumentation umbilical to form a service loop inside the fairing, under the pivot carriage assembly, as shown in figure 6. For the Test 598 configuration ± 11.7 in of free vertical travel was achieved.

Appendix C describes the experimental methods used to estimate the friction in the vertical rails and to monitor the health of the LAS.

3.3 Test Configurations

In Test 598, the model was tested in two configurations: heavy and light. The heavy configuration had five of six inboard leading edge masses, all wing fuel weights, and all eight LAS springs installed. The light configuration had no wing fuel masses, two of six inboard leading edge masses, and four LAS springs installed. The total free flying weight of the heavy and light models were 442 lb and 356 lb, respectively.

Table 1. Model boundary conditions, mount system states, and 1st bending mode frequency.

Bndry Cond		Mount State		1st Mode, Hz	
Pitch	Plunge	Pitch	Plunge	Heavy	Light
Fixed	Fixed	Snub	On Stop	1.9	2.1
Fixed	Free	Snub	Trim	2.0	2.3
Free	Fixed	Trim	On Stop	3.0	3.3
Free	Free	Trim	Trim	3.5	4.1

The boundary conditions and hence, the dynamic characteristics of the wing were altered considerably by the state of the mount system. For instance, when the snubbing system was engaged and the pivot carriage was held on the lower stop via gravity, the wing was essentially cantilevered at the root. The pitch DOF could be freed by releasing the snubber, and the plunge DOF was only free when the model was in trimmed flight. Thus, the mount system provided four distinct boundary conditions that had to be considered. Table 1 shows the various boundary conditions, mount states, and first mode frequency. For the heavy configuration, the frequencies were determined by a ground vibration test performed in the TDT model preparation area, and for the light configuration, frequencies were determined via NASTRAN analysis [12].

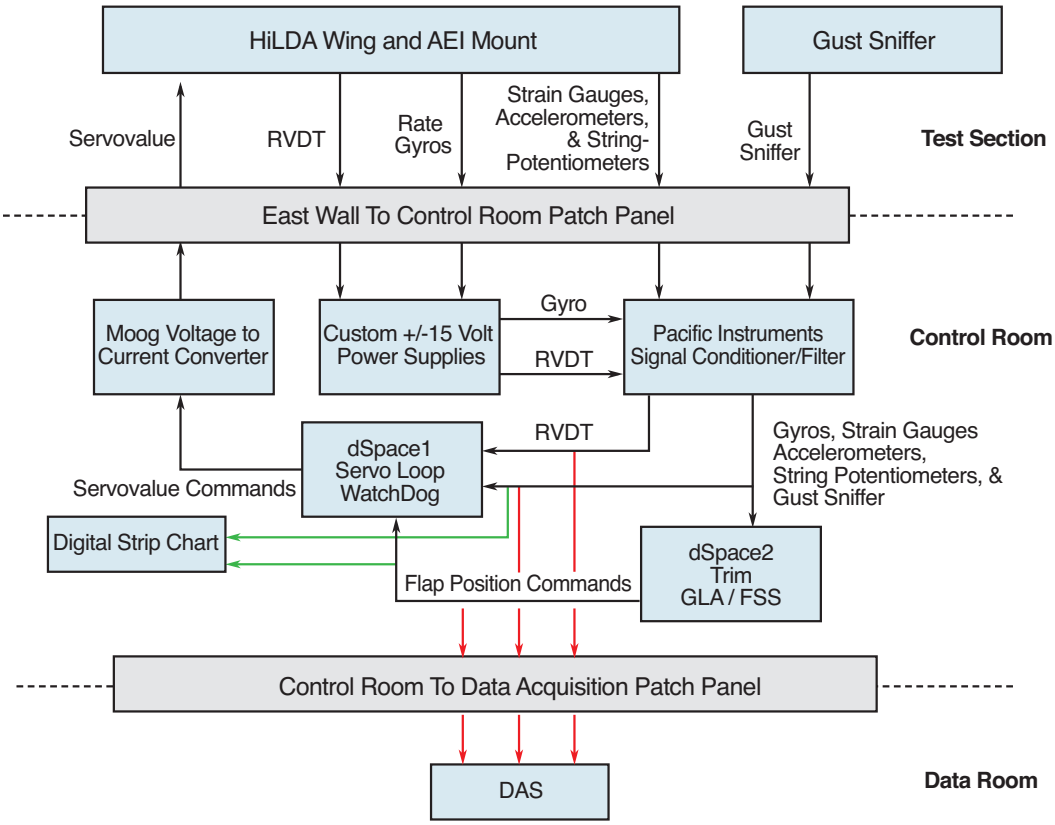

Figure 9. Signal routing used in Tests 593 and 598.

4 Signal Routing, Processing, and Control

Figure 9 shows a high level schematic of the signal routing arrangement used in Tests 593 and 598. All input and output signals were routed from their source to the TDT control room via a built-in wiring system. Most instrumentation was routed to a Pacific Instruments series 6000 chassis that provided instrument power (5 or 10 VDC), signal amplification, and anti-alias filtering. The RVDTs and rate gyros required ±15 VDC power so a custom power supply was fabricated with the signals subsequently routed through the Pacific Instruments chassis for amplification and anti-alias filtering. The anti-aliasing filters were set to 400 Hz for the RVDTs as they were routed only to a digital control system running at a 1,000 Hz frame rate (dSpace1), and all other signals were filtered at 100 Hz to be compatible with the Nyquist frequency for the other digital control system running at a 200 Hz frame rate (dSpace2). Servovalve signals were routed to a Moog voltage-to-current converter and back to the model as shown in the figure. Model signals were "Teed" and routed to a strip chart for monitoring and to the TDT Data Acquisition System (DAS) for recording. The TDT DAS was set to record data at 500 Hz with its own anti-aliasing filters set to 200 Hz.

Figure 10 depicts the snubber control system, dSpace1 and dSpace2 internal block diagrams, and the external signals connecting these systems. All signals external to the dSpace blocks are analog, with dSpace input signals being converted from volts to engineering units prior to processing and output signals being converted from engineering units back to volts. For signals intended to depict discrete system states, programming logic was used to decode the meaning of the signal.

The hydraulic actuators in the snubbing system were operated by a solenoid valve that

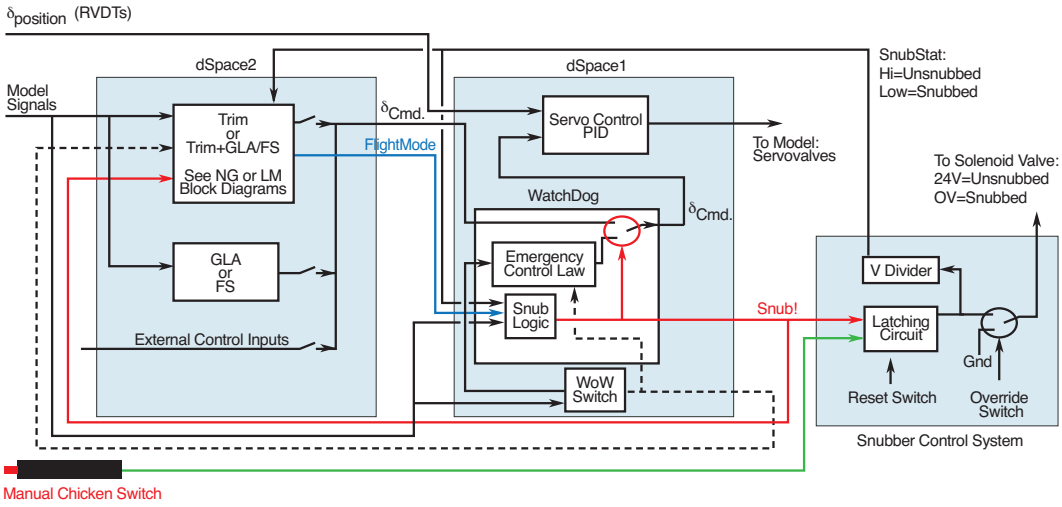

Figure 10. dSpace and snubber control block diagram.

was controlled using the snubber control system. The heart of the snubber control system was a latching circuit that could be tripped by a manual chicken switch or a Snub! command signal from dSpace1. The status of the latching circuit (snubbed or unsnubbed) was communicated back to the dSpace systems by the SnubStat signal in figure 10. A detailed description of the snubber control system and associated hydraulic components is described in a separate section, below.

The trim, GLA, and/or BFF suppression control laws were implemented on dSpace2. Figure 10 shows that dSpace2 had two internal control blocks and a set of externally generated flap commands that could be summed and sent out as analog flap command signals to dSpace1. Throughout most of Test 598, only the upper dSpace2 control block was used with two versions being implemented, one developed by NG and the other developed by LM. This upper control block included a GUI interface and programming logic for controlling or initiating certain events like resetting the system or initiating a launch. Details of the NG and LM flight control architectures, including their associated programming logic, will be described later. The FlightMode state is communicated from dSpace2 to the WatchDog system as shown.

The servo-control loops, the WatchDog system, and the Weight on Wheels (WoW) switch estimator were implemented on dSpace1. The servo-loops were independent PID control loops equipped with output saturation blocks to prevent overdriving the actuators. The WoW switch was a hysteresis block intended to provide debounce or noise tolerance. The WatchDog system monitored the model signals, and when a fault was detected, it would issue a Snub! command and transfer flap control to the emergency control law via the switch shown in figure 10.

Details of the dSpace hardware and software development environment will be described next, followed by a description of the hydraulics and snubber control system.

4.1 DCS Hardware and Development Environment

Each dSPACE DCS consists of a rack containing a host computer, a target system, a keyboard, a monitor, BNC patch panels for IO, and an uninterruptible power source. The heart

of the DCS is the target system that includes a dSPACE DS1006 control processor board using a 2.6 GHz AMD Opteron processor connected to three dSPACE DS2002 multi-channel A/D boards and one dSPACE DS2sec103 multi-channel D/A converter board. The A/D boards each have 32 channels using 16 bit quantization with an input range of ±10 V. The D/A board contains 32 channels of 14 quantization bits designed for ±10 V and a settling time of 10 μs.

The controller software was developed within the MATLAB® Simulink environment, then compiled and downloaded to the target processor via the dSPACE and MATLAB® Real-Time Interface. An integral component of the dSPACE tools is the ControlDesk application which provides the user interface to the target processor for the development and implementation of the GUI. The host computer runs the GUI and controls all communications between the processors.

4.2 Hydraulics and Snubber Control System

Hydraulic control of the pitch snub mechanism was accomplished using a custom snub control system housed in a chassis located in the TDT control room and a hydraulic manifold assembly located in the TDT plenum near the wind tunnel model and mount. Hydraulic fluid, at 2,000 psi, was delivered to the hydraulic manifold assembly from the TDT 30 GPM pump. The manifold assembly consisted of an adjustable pressure switch, a Parker Hannifin solenoid valve, and two regulators for supplying up to two lower pressures to the wind tunnel model. Hydraulic pressure transducers were included to monitor the supply/snub pressure as well as the two regulated pressures. The solenoid valve was normally open and required 24 VDC power to remove pressure from the snubbing system thereby releasing the model.

The snub control chassis served two purposes, monitoring of the hydraulic systems and enclosing the snub control system. The chassis housed three hydraulic pressure displays showing supply/snub pressure and up to two lower, regulated model pressures. An amber light and an audible alarm were wired to the pressure switch to provide warning of reduced hydraulic pressure. The snub control system consisted of two mechanically latching relays that were used to send 24 VDC to the hydraulic solenoid valve. The relays had their contacts wired in series so that either relay could cut the 24 VDC power to the hydraulic solenoid and independently snub the model. One relay was switched directly by the normally open hand-held chicken switch, and the second relay was switched by a voltage signal from an external source.

Figure 11 shows the snub control chassis and a handheld chicken switch. Two amber colored lights on the front of the snub control box indicated which source initiated the Snub! command, either the chicken switch or the external source (WatchDog system). Resetting of the relays and lights was accomplished with a momentary toggle switch (reset switch). There was an independent toggle (override) switch to hold a snub condition which was used to keep the model in a snubbed condition independent of the status of the relays allowing systems to be reset without inadvertently cycling the snub system.

5 WatchDog System

Due to the high risk associated with aeroelastic wind tunnel testing, a variety of manual and automated safety systems have been used in the TDT. The manually operated tunnel bypass valves are generally the first line of defense for flutter testing as they can rapidly reduce test section dynamic pressure and Mach number. Depending on the type of model and mount system employed, model stabilization or arrestment mechanisms have also been considered. Previously employed model stabilization devices have included decoupler pylons that change model dynamics to a more benign configuration and model arrestment devices

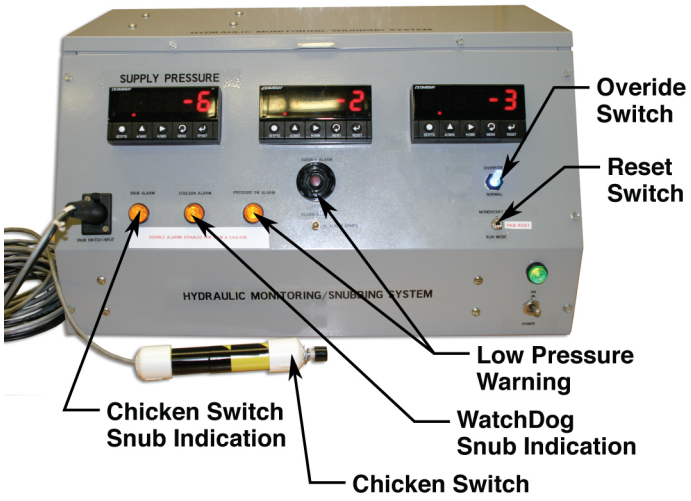

Figure 11. Snub control chassis containing the snub control system with manual Snub! switch and hydraulic pressure displays.

including pneumatic snubber cables for cable mounted models. Manual engagement of these devices has, at times, been supplemented by automated systems. Such systems have previously been employed only for non flying models with the tunnel bypass valves and/or decoupler devices being triggered based on threshold exceedences [14].

The range of rigid body motion and the potential for high speed impact afforded by the new mount system made the AEI flying wing tests among the riskier tests conducted in the TDT. The snubber mechanism was intended to reduce risk to the model and facility, and could be triggered manually. However, human reaction times for "simple" tasks like the sheep dash game in reference 15 are only around 0.22 s, and more advanced tasks, like dodging a baseball, requires a full 0.4 s [16, 17].

In the tunnel testing environment, the test engineer must in essence perform system identification in real time to determine whether a behavior is a benign oscillation or a potentially fatal divergence, mix in a little hope, and the reaction time can be significant. This point is driven home by the worst overload case from Test 593 where the automated system was not used. Figure 12 shows the time histories for vertical position, pitch angle, and inboard bending moment acquired during a failed model launch attempt. For this data point, the peak bending moment significantly exceeded the design load of 15,000 in-lbs with the peak load preceding the manual Snub! command. Clearly, a robust automated system was necessary, so the WatchDog system was developed.

The WatchDog system was developed to keep the model and mount system from exceeding structural safety limits by monitoring signals from the wing and mount system. Difficulty in updating limits and a large number of false positives limited WatchDog use in Test 593. By Test 598, the need for an improved WatchDog system was well established and the deficiencies of the previous implementation were corrected. The system was also expanded to satisfying the differing needs of both Northrop Grumman and Lockheed Martin.

The WatchDog was implemented on dSpace1 as shown in figure 10. The key features of the WatchDog system are the emergency control law and the snub logic. The snub logic monitors the model signals and issues a Snub! command when a fault is detected. Issuing the Snub! command engages the pitch snubber and switches model flap control from dSpace2 to the emergency control law. The subsections that follow will describe the emergency

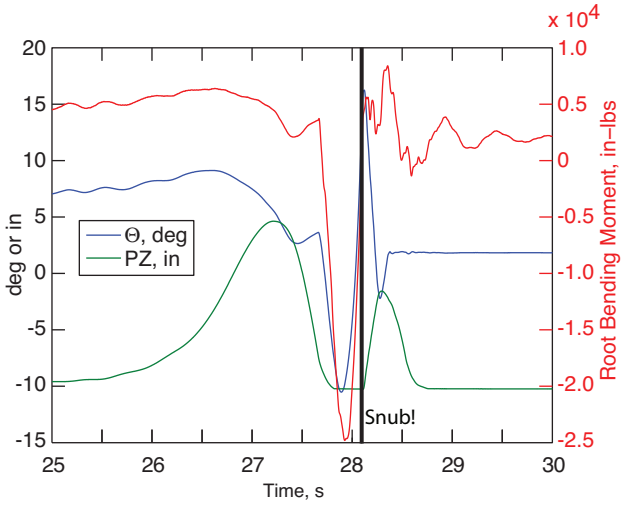

Figure 12. Worst case overload condition from Test 593, point 1833. The bending moment is measured from strain gauge SBI1 shown in figure 8 corrected for outboard wing weight.

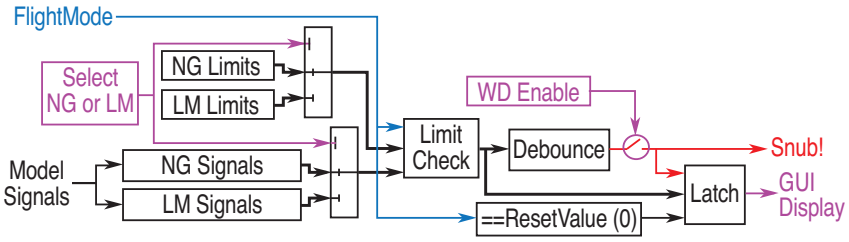

Figure 13. WatchDog system snub logic block diagram.

controller, the snub logic, and some enhancements and unique features that were developed for use by Northrop Grumman and Lockheed Martin for Test 598.

5.1 Emergency Controller

When the model is snubbed, the aerodynamic lift becomes a function only of the dynamic pressure and control surface position, as the model is held at constant angle of attack by the snubbing mechanism. In the snubbed condition, the flaps can be used as lift-only devices. As a result, a simple emergency controller could be developed to arrest the vertical motion and safely land the model after the Snub! command had been issued.

The emergency controller flew the model in the snubbed condition using vertical position error and vertical velocity feedback. The controller gains were divided by the measured dynamic pressure to produce a controller that worked over the dynamic pressure range of interest. The controller also had a flap bias term (δ_o) consisting of the expected control surface positions that would provide total wing lift equal to net wing weight which was the actual wing and pivot carriage weight less LAS force. These bias values were also a function of dynamic pressure, and were initially determined by simulation and then updated as part of the testing process. This testing process will be described later in the paper.

5.2 WatchDog Snub Logic

Figure 13 shows a block diagram of the WatchDog snub logic. The system's primary function was to monitor the 32 model signals and issue the Snub! command when parameter limits had been exceeded. The WatchDog could be enabled or disabled by the user from the dSpace1 GUI. While rarely disabled during Test 598, the feature was needed to facilitate testing under unique circumstances.

From the dSpace1 GUI, the operator can select either the NG or LM limits and signals to be used with the NG or LM control law architectures, respectively. Both NG and LM signal blocks included the basic set of 32 model signals along with some calculated values called combined parameters. The NG and LM limit sets each included a discrete set of upper and lower parameter limits for each FlightMode. The FlightMode was used to select between the sets of limits, so that a different set could be used for reset, takeoff, flight, or GLA testing. The exact definition of the FlightMode parameter was dependent on which flight control architecture was being used, NG or LM. In either case, when the FlightMode associated with model launch and climb-out was used, the lower model position limits needed to be ignored until the model cleared a certain height (PZ value). NG accomplished this by having a separate FlightMode and WatchDog limit set for take off and climb out. LM did not use a separate FlightMode and WatchDog limit set, but instead had some coded logic built into the LM Signals block that ignored the lower position parameters until a certain PZ value had been reached. A more detailed description of these processes will be provided in the flight control schemes section of the paper.

The selected signals and FlightMode dependent limits were compared in the Limit Check block in figure 13. Detected faults were passed to the Debounce block where three consecutive frames of any particular signal fault were required to issue the WatchDog Snub! command. This prevented a single frame noise event from issuing a false alarm. A latch was used to quickly diagnose the cause of WatchDog-commanded Snub! events. The parameter that caused the trip would be held and displayed to the user via the GUI on dSpace1. The WatchDog latch was reset by setting the FlightMode to zero.

Preliminary modeling and review of past tests allowed for initial values of the WatchDog limits to be set. As the wind tunnel test progressed, some limits were expanded based on operational experience. For example, as lower frequency gusts were tested, vertical velocity and pitch rate became large exceeding initial WatchDog limits, but since model response remained stable and bounded, the WatchDog limits were expanded to permit testing. During testing, the limit values could be modified directly in the real time processor memory from the dSpace1 user interface. These modifications were then recorded back into MATLAB® script files for future use.

5.3 NG—Combined Parameters

Based on the WatchDog system deficiencies identified during Test 593, Northrop Grumman proposed that combined parameters be considered in addition to nominal set of 32 model signals. For example, if the model had negative vertical position (below tunnel centerline) and positive vertical velocity (moving up), that would be acceptable. Alternatively, the combination of negative position and negative velocity would be cause for concern. Thus, multiplying vertical position (PZ) and vertical velocity(VZ) produced a parameter that was acceptable when negative and given a safe upper limit and monitored by the WatchDog, i.e. $-\infty < \text{PZ} \times \text{VZ} < \text{limit}$. An additional parameter of $\text{PZ} \times \text{VZ}^2 \times \text{sign(VZ)}$ was also used and was a good indicator of dangerous conditions. These combined parameters increased model safety and provided relatively few false alarms. The NG combined parameters were implemented within the NG Signal block in figure 13. The NG combined parameter limits were set initially by simulation and then modified throughout the test as

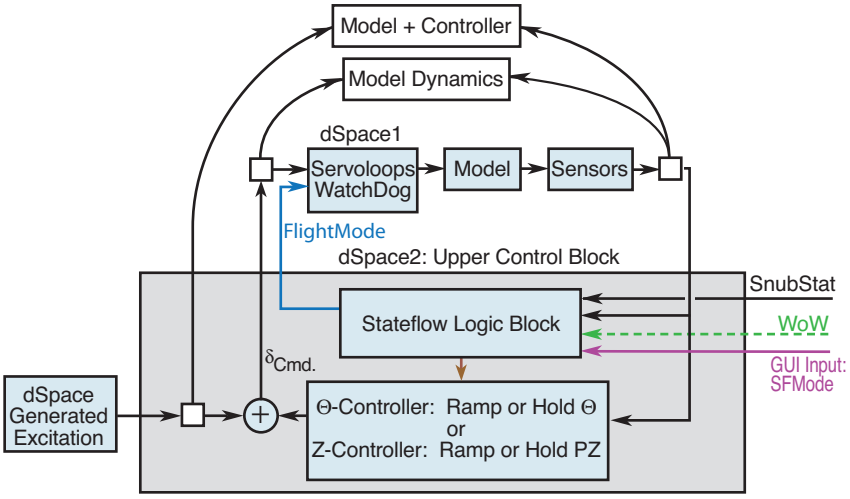

Figure 14. Control law and FlightMode logic developed by Northrop Grumman.

deemed necessary by the test team.

5.4 LM—Combined Parameters

A different set of combined parameters was developed by Lockheed Martin based on an estimate of the vertical location up and down where the emergency controller can bring the model to a stop once the snubber had been engaged for a given vertical speed. These two combined parameters were generated by a feedforward estimator in series with a neural network implemented within the LM Signal block in figure 13. Appendix D provides a detailed description of the simulation model, neural network, and Test 593 data analysis used to develop and validate the LM combined parameters.

6 Flight Control Schemes

Two schemes for achieving trimmed flight were developed and demonstrated: the TakeOff and the Release schemes developed by Northrop Grumman and Lockheed Martin, respectively, with the assistance of NASA Langley Research Center. The TakeOff scheme simulates a take-off roll, acceleration, rotation, and lift-off. Alternatively, the Release scheme kept the model snubbed until flight speed was achieved in the tunnel, then it was unsnubbed and lifted off. This section will describe each launch scheme and its associated control law architecture. Example wind tunnel data will be provided where appropriate.

6.1 Takeoff Launch Scheme

The TakeOff launch scheme approximates an aircraft takeoff process beginning with a high speed ground roll, followed by rotation, lift-off, climb, and finally, trimmed flight. Figure 14 shows the control law architecture associated with the TakeOff launch scheme. As shown in the figure, the TakeOff launch scheme makes use of the MathWorks Stateflow package. Stateflow extends Simulink with a design environment for developing state machines and flow charts. The NG implementation of Stateflow allows most TakeOff launch scheme actions to be event-driven. The Stateflow Logic Block is controlled by the Stateflow Mode (SFMode) parameter via the dSpace2 GUI as indicated.

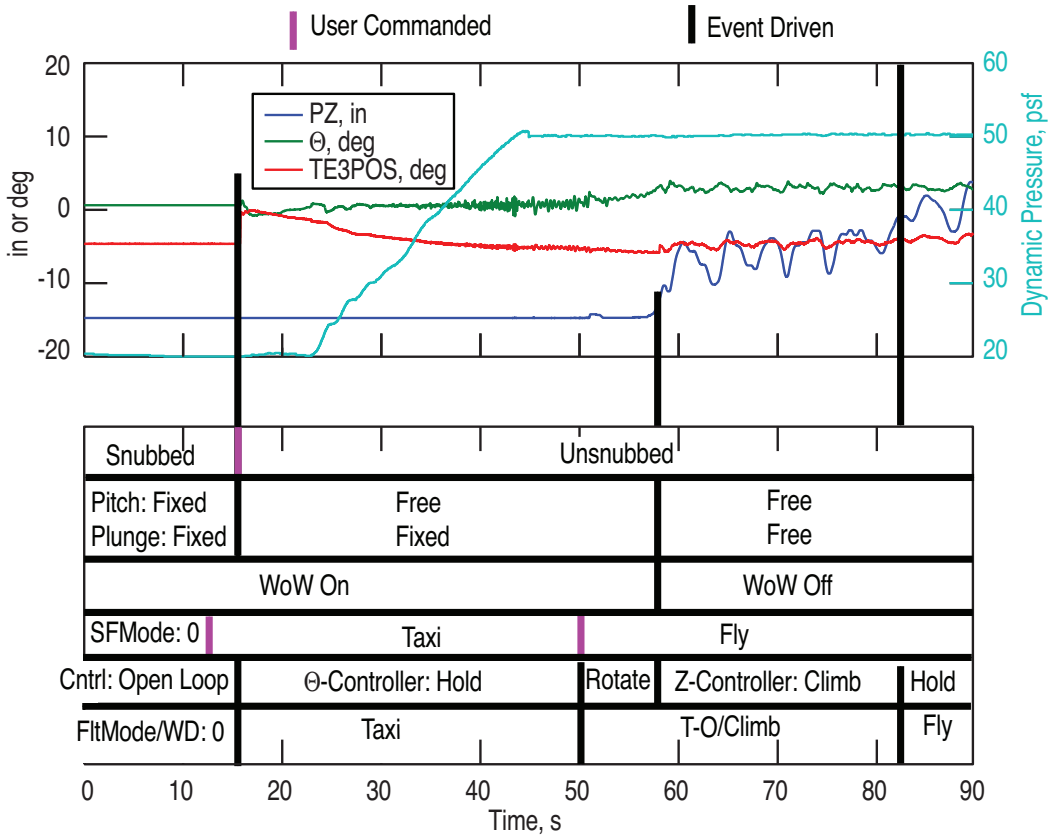

Figure 15. Data acquired while using TakeOff launch scheme to achieve trimmed flight. Test 598, points 1274, 1275, and 1276.

The TakeOff launch scheme requires two separate controllers. A Θ-controller is used during the pitch-free condition when the model is on the lower vertical stop, and a Z-controller is used when the model takes off and transitions to the free-free boundary condition. These control laws were developed using the LQG method and incorporated GLA and trim control into a single controller. This allowed studies to be performed that directly traded short period performance with GLA performance. Reference 18 discusses the design of these controllers and their initialization methods in more detail.

Figure 15 shows data acquired during implementation of the TakeOff launch scheme. Here, time histories of PZ, Θ, TE3 position, and dynamic pressure are plotted in the upper part of the figure, and the timing of boundary condition changes, Stateflow modes, and other system states are identified in the lower portion of the figure. User- and event-driven actions are identified. This figure should be consulted when reading the following TakeOff launch scheme steps:

T = 0 s: Start with model snubbed, dynamic pressure set to 20 psf, and SFMode set to 0. Stateflow sets FlightMode to 0 telling the WatchDog to use the reset limits.

T = 13 s: The operator sets SFMode to Taxi. Controller is ready and waiting to detect the unsnubbing of the model via the SnubStat signal from the snubber control system.

T = 15 s: The operator unsnubs the model using the reset switch on the snubber control system chassis. Stateflow senses the unsnub condition via the SnubStat signal and initiates the Θ-controller holding a constant 1° set point. It also changes FlightMode

to Taxi telling the WatchDog system to use the Taxi limits.

T = 24 to 45 s: Dynamic pressure is increased to the launch value of 50 psf.

T = 50 s: The operator sets SFMode to Fly. Stateflow then starts the Θ set-point ramp, i.e. rotation, and changes FlightMode to T-O/Climb telling the WatchDog system to use the T-O/Climb limits.

T = 58 s: The model lifts off the lower stop and passes through the WoW switch causing Stateflow to transition from the Θ-controller to the Z-controller. The PZ set point for the Z-controller is ramped up causing the model to climb. Also, as the WoW switch is cleared, the model boundary conditions transition to free-free.

T = 83 s: Stateflow senses that PZ has reached a value of -1 in and changes the PZ set point to the tunnel centerline value of 0. Stateflow also changes FlightMode to Fly telling the WatchDog system to use the Fly limits.

T > 90 s: Dynamic pressure is increased, as necessary, to the desired test condition. Operator can set SFMode to Test. Stateflow then changes FlightMode to Test which tells the WatchDog system to use the Test limits. When testing is complete, the snubber chicken switch is used to manually engage the snubbing system and land the model using the emergency control law.

This method was shown to be successful and led to a better understanding of the model in early testing. However, the large dynamic pressure changes that were required for each launch made it very time consuming. In addition, the pitch-free boundary condition is not very stable and is significantly more difficult to control than the free-free boundary condition. As a result, engineering effort had to be used to develop stable Θ-controllers. Also, the transition from the Θ-controller to the Z-controller must have a small enough transient not to overly perturb the model. Thus, the Z-controller bandwidth and performance was being driven by the need to mitigate the takeoff transition. While this challenge is understood and manageable in conventional flight control architectures, it presents particular challenges when investigating large state-space controllers.

6.2 Release Launch Scheme

For the Release launch scheme, the control surfaces were prepositioned for flight prior to releasing the pitch snub mechanism so that when the snubber was released the model flies off the bottom stop. The model transitions from the stable fixed-fixed boundary condition to the stable free-free conditions without dwelling at the unstable pitch-free condition. This quick transition does not allow the unstable pitch-free configuration to build up any response amplitude. Therefore, there was no need to control the pitch-free configuration using a Θ-controller.

The control architecture used with the Release method was a two-loop system as shown in figure 16. The inner loop contained the trim controller and was responsible for flying the model, and the outer loop contained the suppression controller and was responsible for reducing the dynamic response. The suppression controller could be switched on and off with little or no effect on the average control surface trim position. As a result, switching between controllers caused little trim/elevation change and was done frequently throughout the test to acquire GLA data with as many controllers as possible without having to repeat the launch procedure.

The trim controller consisted of vertical position PID gains plus a pitch rate gain and a static (bias) term. The proportional and integral terms were ignored until the model was unsnubbed. The output of the trim controller was a single command that was sent to all four trailing edge flap surfaces. The trim controller gains were initially established from analysis, and a single set of trim controller gains were identified that were applicable to both the heavy and light model. The bias term and the dynamic trim gains could be adjusted

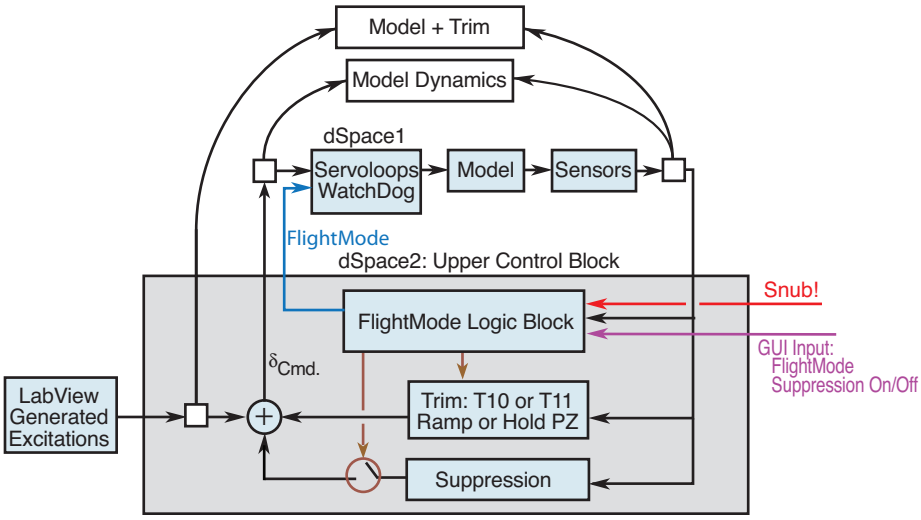

Figure 16. Trim and suppression control loops along with FlightMode logic developed by Lockheed Martin.

from the dSpace2 GUI. Two versions of the trim controller were used during Test 598; T10 and T11. Trim controller T11 was better suited to TDT testing with the AOS system operating.

The suppression controllers were developed utilizing the system identification and LQR/LQG techniques described in reference 19. System identification data were acquired around the inner loop, as indicated by the lines in figure 16, providing the model and model plus trim controller system dynamics. These system identification data were then used with the LQR/LQG methods to build the suppression controller. Therefore, the suppression controllers were aware of and expected the trim controller to be part of the system. Reference 20 covers this subject in more detail.

As with the TakeOff launch scheme, the WatchDog limits associated with the Release launch scheme had to be set to ignore the lower position limits during the launch and climb out phase of flight. For the TakeOff launch scheme, the logic for ignoring lower vertical limits was contained entirely within the Stateflow logic block, and a separate set of WatchDog limits was selected for this phase of flight. For the Release launch scheme, a separate FlightMode for launch and climb out was not used. Instead, logic was built into the LM Signal block shown in figure 13 that ignored certain parameters until PZ had reached a value of -7 in. Another difference between the two launch schemes is that in the TakeOff launch scheme the operator sets the SFMode parameter via the GUI, but FlightMode is event-driven via the Stateflow logic block. When using the Release launch scheme, the operator sets the FlightMode directly via the GUI.

For the Release launch scheme, FlightMode 0 was a reset mode, FlightMode 1 was a trim control only mode, and FlightMode 2 allowed the use of the suppression loop. Each FlightMode had a different set of WatchDog limits. FlightMode 1 was used for launch and climb out, so parameters that would snub the model when it was on the lower stop were ignored until PZ reached a value of -7 in. To protect the model during takeoff, in FlightMode 1 the WatchDog Θ lower limit was set to 0° to minimize the possibility of a pitch over and subsequent hard landing event.

Figure 17 shows data acquired during implementation of the Release launch scheme. Here, time histories of PZ, Θ, TE3 position, and tunnel dynamic pressure are plotted in

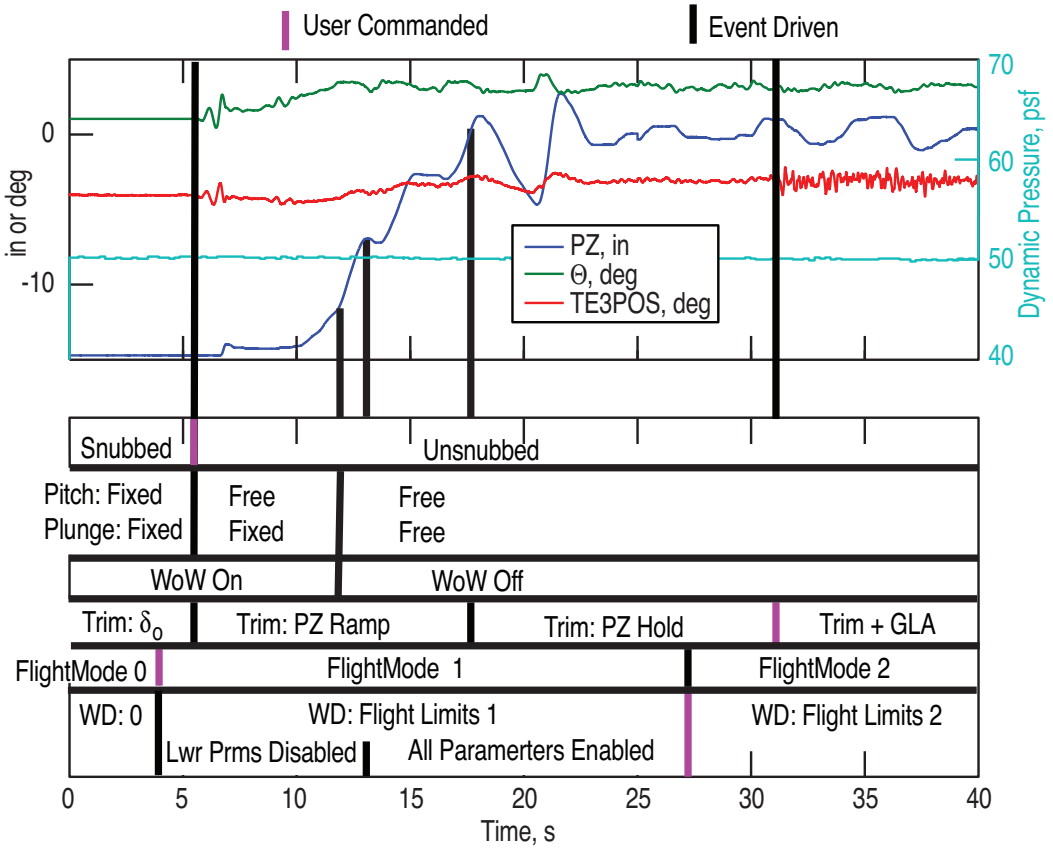

Figure 17. Data acquired while using Release launch scheme to achieve trimmed flight. Test 598, point 2384.

the upper part of the figure, and the timing of boundary condition changes, FlightMode changes, and other system states are identified in the lower portion of the figure. User- and event-driven actions are identified. This figure should be consulted when reading the following Release launch scheme steps:

T = 0 s: The model is snubbed. Tunnel dynamic pressure is set to the launch value of 50 or 60 psf. FlightMode is set to zero by the operator causing the control surfaces to be pre-positioned by the static part of the trim controller (δ_o). This also puts the WatchDog in reset mode (0) which resets the latching logic associated with the lower position limits in WatchDog limit set 1.

T = 5.5 s: The operator unsnubs the model using the reset switch on snubber control system chassis. The FlightMode logic block within the LM flight control architecture senses the unsnubbed condition via the Snub! command signal and initiates the dynamic part of the trim controller. The PZ set point for the trim controller begins ramping to tunnel centerline. The model starts to rotate but does not immediately lift off. This is an unstable condition, and the model starts to oscillate in pitch.

T = 7 s: The model lifts off the bottom hard stop but is supported on the extended shocks. The integral part of the trim controller continues to increase the control surface deflection and Θ.

T = 12 s: The model clears the WoW switch indicating that it is off the shocks and has transitioned to the free-free boundary condition. This event does not trigger any action within the Release scheme and associated LM control architecture.

T = 13 s: The vertical position passes through -7 in and the WatchDog begins monitoring all signals including the lower vertical limits.

T = 17.5 s: The PZ set point for the trim controller reaches and holds the tunnel centerline value (PZ = 0).

T = 27 s: FlightMode is manually changed to FlightMode 2 which allows the use of the suppression control law but does not close the suppression loop.

T = 31 s: A suppression controller is engaged by the operator via the dSpace2 GUI. The higher frequency control surface activity is associated with the suppression loop being closed.

T>40 s: Dynamic pressure is increased, as necessary, to the desired test condition. When testing is complete, the snubber chicken switch is used to manually engage the snubbing system and land the model using the emergency control law.

The Release launch scheme proved to be easy, effective, and insensitive to dynamic pressure and model configuration.

7 Testing Procedures

With the exception of several air checkout runs, all Test 598 data was acquired in heavy gas with a tunnel total pressure between 1,670 and 1,880 psf. This maps to a fairly tight band of Mach number and dynamic pressure combinations as shown in figure 18 where a portion of the TDT heavy gas operating envelope is shown along with the Test 598 data points. At any given tunnel total pressure, Mach number and dynamic pressure are not independent of each other and vary in unison with changes in the RPM of the TDT main drive motor. For the test procedure of Test 598, increasing RPM varied tunnel conditions along the plotted data points starting with the lower left. As Mach number is relatively insensitive to tunnel RPM in this region, dynamic pressure was used to identify all tunnel conditions.

As previously mentioned, the model and mount system had four testable boundary conditions. Data presented in table 1 shows that the first bending mode frequency changed significantly based on these conditions, and as a result, model flutter speeds varied with

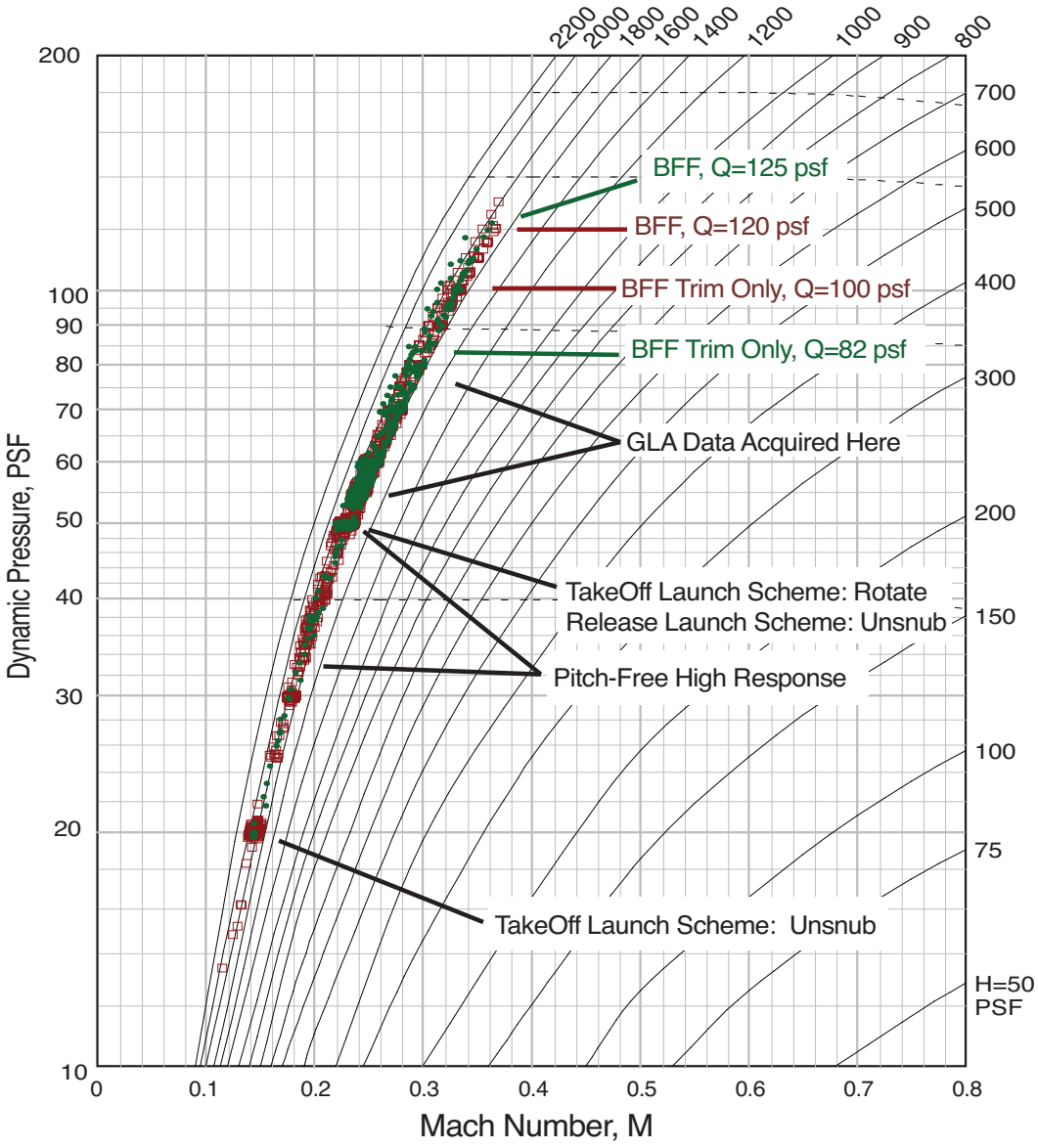

Figure 18. Portion of the TDT heavy gas operating envelope showing data acquired during Test 598 where red represents the heavy weight configuration and green represents the light weight configuration.

snub and flight status. Due to the possibility for high speed vertical impact, the riskiest configuration was with the model in a free-free, flying configuration. The safest configuration was with the pitch DOF snubbed and the model sitting on the lower stop. For both the heavy and light configurations, the relatively safe configurations were cleared for flutter and the functionality of the emergency controller verified prior to proceeding with free-free flight at a given dynamic pressure. The subsections that follow will describe the various test procedures in general order of increasing complexity.

7.1 Open-Loop Flutter Clearance

The model and mount system could be tested open-loop when the pivot carriage was sitting on the lower mount with and without the pitch snub mechanism engaged. Flutter clearance testing of these configurations was performed in a manner typical of TDT flutter testing. Dynamic pressure was increased slowly while the model was monitored visually and its signals monitored via strip chart.

For the fixed-fixed case, flutter clearance was somewhat pro forma, as this configuration had the least modeling unknowns and the highest analytical flutter speeds [5]. Also, it had previously been tested in this configuration (Test 579 and Test 593) up to a dynamic pressure of at least 80 psf. During Test 598, the fixed-fixed configuration was only cleared for flutter to a dynamic pressure of 60 psf. The high degree of confidence in the analysis and the concern that the model would not remain on the lower stop during this testing due to the fixed, positive, snub pitch angle precluded flutter clearance testing above 60 psf.

The other open-loop configuration that was tested for flutter was pitch-free with the model on the lower stop. This configuration required that the model be manually trimmed to keep pitch angle from getting too large causing the model to lift off the lower stop. This configuration was of interest because it was the model boundary condition state for the Taxi mode in the TakeOff launch scheme. The exact flutter onset dynamic pressure was somewhat ambiguous for this configuration as this flutter mechanism appeared to be a hump mode with a very shallow flutter crossing. Experimentally, this was demonstrated by an inconsistent flutter dynamic pressure and a relatively benign flutter mechanism. This behavior occurred at dynamic pressures between 30 and 50 psf.

7.2 Snubbed Flight Clearance and Emergency Controller Validation

The next stop on the way toward achieving trimmed, free-free flight was to verify and tune the emergency controller. The purpose of the emergency controller was to gently return the model to the lower stop using gains and biases scheduled with dynamic pressure. The bias values had to be adjusted based on experimental data. An additional purpose of this testing was to simultaneously verify that the model was flutter free in the snubbed flying configuration up to the maximum expected dynamic pressure of interest.

The process for clearing the model for flutter was to fly the model in the snubbed configuration at tunnel center line (PZ = 0) and incrementally increase dynamic pressure stopping approximately every 10 psf. Once aeroelastic stability had been established, controller validation data was acquired using the emergency controller to track a sawtooth position command between -10 in and $+10$ in with a ramp rate of ± 1 in/s. Data was acquired for three complete saw tooth cycles. The average control surface position needed to fly the model at each dynamic pressure was determined and used as the static component (δ_o) of the emergency controller.

In preparation for GLA testing this clearance/validation process was performed from the takeoff dynamic pressure of 50 psf to 70 psf, the maximum dynamic pressure where GLA data would be acquired. In preparation for BFF testing, the process was repeated for

dynamic pressures above 70 psf to a maximum dynamic pressure of 130 psf. The testing process had to be repeated for the light model.

7.3 Gust Load Alleviation Testing

So far, this paper has described the apparatus, procedures, and preliminary testing that were necessary to achieve trimmed, free-free flight in a safe and predictable manner. Demonstrating that a control law reduced loads due to gusts required that data be acquired using different control laws all in the same gust environment. Here, the acquisition of the GLA data with the TDT AOS operating will be discussed.

The biggest problem encountered with AOS testing was simply to get the model in a trimmed flying state with the AOS operating. Initial attempts failed when the model was first launched into a stable, trimmed flight condition prior to turning on the AOS. The AOS uses a large flywheel to hold constant vane frequency, and therefore, changes in frequency occur relatively slowly. As a result, when the AOS system was engaged, the model encountered a low frequency sinusoidal gust field with flow angles of approximately $\pm 1^\circ$ (at the initial AOS amplitude setting of 12° peak-to-peak). The vertical travel required for the wing to fly through this gust field exceeded the vertical travel available on the mount system, and the WatchDog system or test engineer would snub the model. The solution to this problem was to bring the AOS on-line prior to launching the model. An AOS frequency well above the rigid body modes and between the resonant frequencies of the flexible modes (firstin-plane and second out-of-plane bending) was used, typically 6.5 Hz. This technique allowed both the TakeOff and Release launch schemes to be successfully used.

An interesting aside regarding the AOS is that on several occasions launch sequences that had previously been successfully employed failed to work. In these instances, the model would fly to the top of its vertical travel and trip the WatchDog system. It was determined that the AOS vanes had been parked at a nonzero angle, and this flow angularity change was enough to cause the model to fly to its upper travel limit during launch attempts. Re-zeroing the AOS vanes solved the problem.

For the Release scheme, it was experimentally determined that trim controller T10 could only be used during model launch with the AOS off. Thus, the trim controller gains had to be adjusted slightly in order to successfully launch the model when the AOS was operating. Two versions of the Release scheme trim controller were ultimately used, the AOS and non-AOS versions or T11 and T10 trim controllers, respectively. The higher gains and initial control surface position in T11 provided a snappier launch and better position tracking. Although T11 could be used to launch the model with and without the AOS operating, this was generally not done as T10 was the preferred baseline controller for the AOS off cases.

In the case of the TakeOff scheme, the same control laws could be used to launch with and without the AOS operating. Since trim and GLA were combined for the TakeOff scheme, the inherent disturbance rejection associated with GLA may have allowed these control laws to achieve this without any special AOS related design considerations.

At this point, the differences between the control law design methods associated with the TakeOff and Release schemes dictated how the testing for each was conducted. For the TakeOff scheme, the trim/GLA controllers were designed using state-space analytical models. LQG methods were employed where the weightings were varied to produce different controllers that provided various levels of GLA performance, and many such controllers were evaluated. The GLA evaluation procedure consisted of acquiring model response data for each control law subject to AOS dwells in 0.5 to 0.1 Hz frequency increments. Generally, this type of testing would start at a relatively high AOS frequency and proceed to lower frequencies until the WatchDog or test engineer snubbed the model. When the model was snubbed, the AOS operator would return to the system to 6.5 Hz to reduce the large amplitude wing bending oscillations associated with peak response frequencies and to prepare

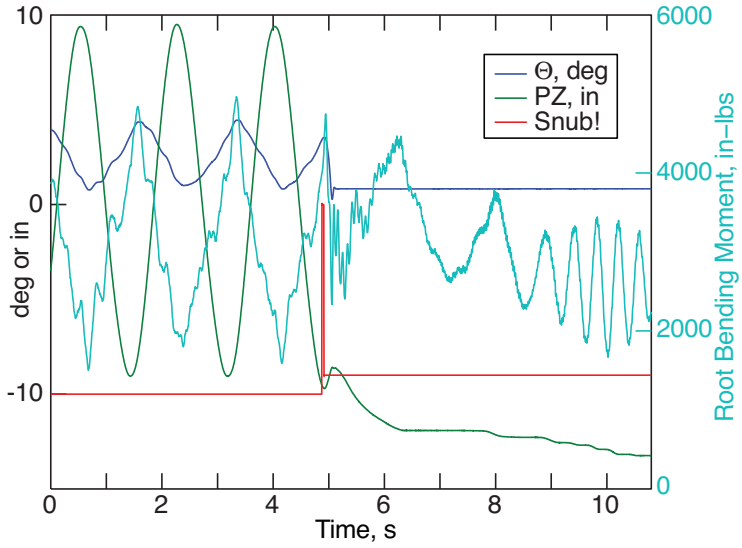

Figure 19. Time traces of vertical position, pitch angle, and bending moment while AOS transitioning from 0.7 to 0.5 Hz. WatchDog Snub! engagement shown along with subsequent vertical position ramp down. Test 598, point 4891. The bending moment was measured from strain gauge SBI1 (figure 8) corrected for outboard wing weight.

for another launch using a different control law. Figure 19 provides some example data where the AOS frequency was about 0.6Hz. Here, the vertical displacement is quite large approaching ±10 in. At T = 4.9 s, a WatchDog limit was exceeded and the model was snubbed and returned to the lower stop by the emergency controller.

When using the Release launch scheme and associated LM controller architecture, a system ID approach was used to generate the GLA controllers. The system ID data was acquired with uncorrelated random excitations sent simultaneously to each flap. These excitations were generated externally using a LabVIEW® system with the excitations added to the flap commands within dSpace2 as shown in figure 16. As discussed earlier, the system ID data needed to capture the model with the appropriate trim control loop engaged.

Acquisition of system ID data for use when the AOS was not engaged was relatively straight forward. However, a new procedure had to be developed to generate system ID data for generating GLA controllers for use with the AOS engaged. Here, the external frequency command feature of AOS was used with the LabVIEW® system to sweep through the frequency range of interest. Typically, this was from an upper frequency of 9.5 to 11 Hz down to a frequency slightly above where the model was expected to exceed WatchDog limits then back to the upper frequency. The random excitations were simultaneously sent to the flaps while the AOS system was sweeping.

Suppression controllers generated using these data could be evaluated using the AOS dwells, described earlier, or the AOS sweep excitation without the random flap inputs included. Figure 20 shows time traces acquired during an AOS sweep. Here, the AOS frequency is varied from 9.5 to 2.0 back to 9.5 Hz during a 100 second data record. Large bending moment and plunge displacement responses were obtained at the low AOS frequencies.

The lowest frequency that could be obtained using either the AOS dwell or sweep excitations was a function of dynamic pressure. For the heavy model and a dynamic pressure of 70 psf, the WatchDog system would generally trip between 3.0 and 2.5 Hz, and at 60 psf

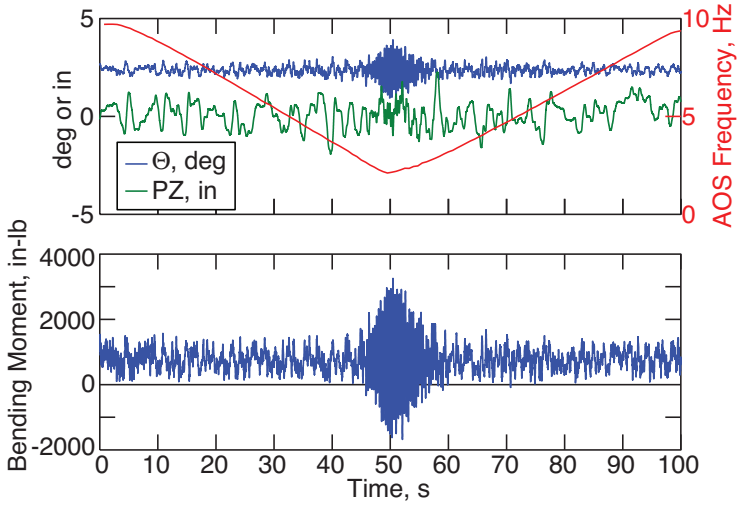

Figure 20. Time traces of vertical position, pitch angle, and bending moment while AOS sweeping from 9.5 to 2.0 to 9.5 Hz. Test 598, point 3182. The bending moment is measured from strain gauge SBI1 (figure 8) corrected for outboard wing weight.

it would typically trip between 1.7 and 2.5 Hz. The actual lower limit was a function of the specific controller engaged at the time. Similar trends were noted for the model in the light configuration. For the final week of testing, the peak-to-peak amplitude of the AOS vanes was reduced from 12° to 4°. Following this change, data could be acquired with AOS frequencies below 1.0 Hz for dynamic pressures of 60 psf as previously shown in figure 19.

References 18 and 20 show more details on the GLA control laws and associated experimental results.

7.4 Reduced Static Margin Testing

The movable mass could be remotely adjusted from the TDT control room during wind tunnel testing. For model launch and most subsequent testing, the nominal location of this mass was full forward for the heavy configuration and full aft for the light configuration. In the heavy configuration, the movable mass and model's CG could be moved aft to investigate reduced static margins. The procedure was to establish trimmed flight with the mass in the nominal (full forward) location and set the dynamic pressure to the desired value. Then the mass was moved aft, incrementally, until the model went unstable and was snubbed or the mass made it to the full aft position. Data was acquired periodically during this process.

7.5 BFF Suppression Testing

For flutter testing, the goal was to establish the experimental flutter onset dynamic pressure associated with a given control law. As with the flutter clearance testing, dynamic pressure was increased incrementally; however, since flutter was expected, the increments were reduced as dynamic pressure was increased into uncharted territory. For this testing, naturally occurring tunnel turbulence was generally deemed adequate to perturb the model, but control surface doublets were occasionally used to free stiction in the mount system. Ultimately, flutter onset was determined by the test engineer's assessment that the model was unstable or when the WatchDog limits had been exceeded. In either case, the model

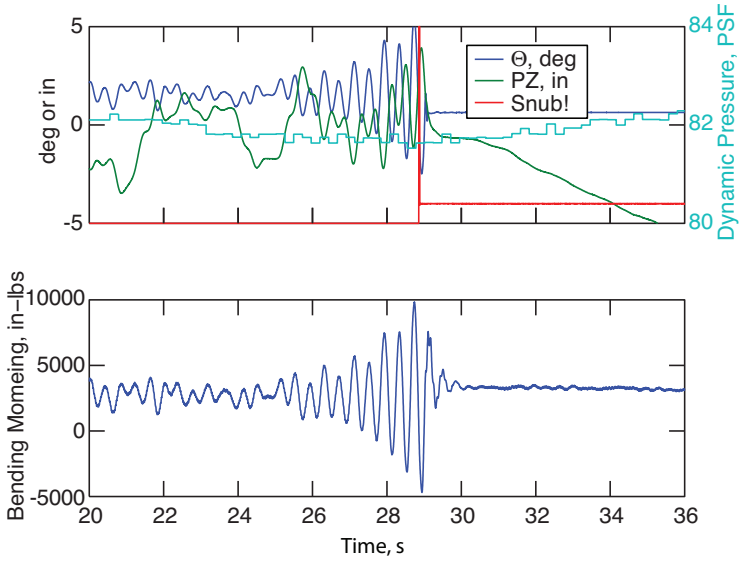

Figure 21. Body freedom flutter time traces for trim only control, light model. WatchDog Snub! engagement shown along with subsequent vertical position ramp down. Test 598, point 3525. The bending moment is measured from strain gauge SBI1 (figure 8) corrected for outboard wing weight.

would be snubbed. Figure 21 shows data from one such BFF encounter where the WatchDog system engaged the snubber and the model was subsequently landed via the emergency controller. Note that Θ and PZ have the same frequency and are growing in amplitude.

Controllers associated with the TakeOff launch scheme were tested past their designed dynamic pressure to determine the onset of BFF. While not a specific test objective of Northrop Grumman, the demonstration of BFF suppression and the system ID data acquired provided a measure of controller robustness and validated flutter onset predictions.

Controllers associated with the Release launch scheme were tested extensively for flutter in the heavy and light configurations. As the objective of this testing was to generate BFF suppression controllers that would increase flutter onset above the trim-controller-only value, a boot strap method had to be employed. The first step was to establish the trim-controller-only (baseline) flutter onset dynamic pressure, acquiring system ID data incrementally as dynamic pressure was increased. These data were then used, off-line, to generate BFF suppression control laws. When testing resumed with the combined trim/BFF-suppression controller engaged, system ID data would again be acquired as dynamic pressure was increased until a new flutter onset value was established. The system ID and control law design procedure was repeated until the maximum value of flutter onset dynamic pressure was established. References 12 and 20 contain more details on the BFF suppression control laws and a discussion of the experimental results.

8 Concluding Remarks

In the Fall of 2007, the Air Force Research Laboratory (AFRL), Northrop Grumman, Lockheed Martin, and NASA Langley Research Center successfully completed the third of a series of three wind tunnel tests of an aeroelastically scaled wind tunnel model of a flying wing SensorCraft vehicle concept. The first of these tests was conducted on a cantilevered,

sidewall mount. The second and third tests used a new, multi-DOF mount. This mount allowed the semi-span model to translate vertically and rotate in pitch at the wing root, allowing better simulation of the full span vehicle's rigid-body modes. The large size of the flying wing model along with the rigid body DOF afforded by the new mount system, created many unique challenges to successfully and safely flying the model in the tunnel and meeting the AEI test objectives. This paper has provided an overview of the AEI flying wing wind tunnel tests from an operational point of view. It has focused on systems, procedures, and lessons learned that enabled the test to be successful in demonstrating Gust Load Alleviation (GLA) and Body Freedom Flutter (BFF) suppression. Descriptions of the hardware including the wind tunnel, the wing model, the mount system, and other supporting systems developed for this program were provided.

9 Acknowledgements

From Northrop Grumman the authors would like to acknowledge Tony Shimko for his expertise and guidance, Elaine Shaw for her tireless control design, test engineers, Lou Scherer, Chris Curnes and Kian Tehrani, and finally, Ted Schulman for much appreciated experience and insight.

From Lockheed Martin the authors would like to acknowledge Wink Baker and David White for their contributions to Test 598 that including model preparation, calibration, and wind tunnel testing.

From NASA Langley Research Center the authors would like to acknowledge Chuck McClish for building the hydraulic manifold assembly, Patrice Quander-Haas and Gary Koepple for fabricating the snub control chassis, the moving mass controller, and their patience in dealing with ever changing requirements, Vic Tumwa for his assistance in conducting ground vibration tests, William Johnston and John Newman for performing the LAS spring fatigue test on such short notice, and Mike Ramey, Jeff Wilfong, and Anthony Pototzky for their assistance in conducting the wind tunnel test.

Finally, we would like to acknowledge the design, fabrication, and test support efforts of NextGen Aeronautics including David Cowan, Matthew Scott, Dana Howard, Robert Alphenaar, Robert Myers, Jonathan Prouty, and Richard Guhr.

References

1. Lucia, D., "The SensorCraft Configurations: A Non-Linear AerServoElastic Challenge for Aviation," *46nd AIAA/ASME/ASCE/ASC Structures, Structural Dynamics and Materials Conference*, Austin Texas, April 2005.

2. Martinez, J., "An overview of SensorCraft capabilities and key enabling technologies," *26th AIAA Applied Aerodynamics Conference*, No. AIAA-2008-7185, Honolulu, Hawaii, Aug. 2008.

3. Reichenbach, E., "Aeroservoelastic Design and Test Validation of the Joined Wing Sensorcraft," *26th AIAA Applied Aerodynamics Conference*, No. AIAA-2008-7189, Honolulu, Hawaii, Aug. 2008.

4. LeDoux, S., Vassberg, J., and Fatta, G., "Aerodynamic Cruise Design of a Joined Wing SensorCraft," *26th AIAA Applied Aerodynamics Conference*, No. AIAA-2008-7190, Honolulu, Hawaii, Aug. 2008.

5. Lockyer, A. J., Drake, A., Bartley-Cho, J., Vartio, E., Solomon, D., and Shimko, T., "HIGH LIFT OVER DRAG ACTIVE (HiLDA) WING; Delivery Order 0007: HiLDA

Wing Program," Tech. Rep. AFRL-VA-WP-TR-2005-3066, Northrop Grumman Corporation, 2005.

6. Vartio, E., Shimko, A., Tilmann, C. P., and Flick, P. M., "Structural Modal Control and Gust Load Alleviation for a SensorCraft Concept," *46th AIAA/ASME/ASCE/AHS/ASC Structures, Structural Dynamics and Materials Conference*, No. AIAA-2008-7185, Austin, Texas, April 2005.

7. Silva, W., Vartio, E., Shimko, A., Kvaternik, R. G., Eure, K. W., and Scott, R. C., "Development of Aeroservoelastic Analytical Models and Gust Load Alleviation Control Laws of a SensorCraft Wind-Tunnel Model Using Measured Data," *47th AIAA/ASME/ASCE/AHS/ASC Structures, Structural Dynamics and Materials Conference*, No. AIAA-2006-1935, Newport, Rhode Island, May 2006.

8. Staff of the Aeroelasticity Branch, "The Langley Transonic Dynamics Tunnel," Langley Working Paper LWP-799, Sept. 1969.

9. Corliss, J. M. and Cole, S. R., "Heavy Gas Conversion of the NASA Langley Transonic Dynamics Tunnel," *Proceedings of the 20th Advanced Measurements and Ground Testing Technology Conference*, No. 98-2710, Albuquerque, NM, June 1998.

10. Cole, S. R. and Rivera Jr, J. A., "The New Heavy Gas Testing Capability in the NASA Langley Transonic Dynamics Tunnel," *Royal Aeronautical Society Wind Tunnels and Wind Tunnel Test Techniques Forum*, No. 4, Cambridge, UK, April 1997.

11. Bartley-Cho, J. and Henderson, J., "Design and Analysis of HiLDA/AEI Aeroelastic Wind Tunnel Model," *26th AIAA Applied Aerodynamics Conference*, No. AIAA-2008-7191, Honolulu, Hawaii, Aug. 2008.

12. Love, M. H. and et al., "Final Report for the Aerodynamic Efficiency Improvement Contract No.: FA8650-05-C-3501," Tech. Rep. FMZ-9454, Lockheed Martin Corporation, 2008.

13. Mangalam, S. and Mangalam, A., "Unsteady Aerodynamic Observable for Gust Load Alleviation and Flutter Suppression," *26th AIAA Applied Aerodynamics Conference*, No. AIAA-2008-7187, Honolulu, Hawaii, Aug. 2008.

14. Perry, B., Cole, S. R., and Miller, G. D., "Summary of an Active Flexible Wing Program," *AIAA Journal of Aircraft*, Vol. 32, No. 1, 1995, pp. 10–15.

15. "http://www.bbc.co.uk/science/humanbody/sleep/sheep/," BBC Homepage, Science & Nature: Human Body & Mind, Sheep Dash! A simple on-line game testing human reaction time.

16. McDowell, M. M., "A Controlled Study on Batted Ball Speed and Available Pitcher Reaction Time in Slowpitch Softball," *British Journal of Sports Medicine*, Vol. 39, 2005, pp. 223–225.

17. "Sanchez v. Hillerich & Bradsby Co." Court of Appeal, Second District, Division 4, California, 2002, http://www.napil.com/PersonalInjuryCaseLawDetail31772.htm.

18. Vartio, E. and Shaw, E., "GLA Flight Control System Design for a SensorCraft Vehicle," *26th AIAA Applied Aerodynamics Conference*, No. AIAA-2008-7192, Honolulu, Hawaii, Aug. 2008.

19. Larimore, W. E., "Optimal Order Selection and Efficiency of Canonical Variate Analysis System Identification," *Proc. 13 IFAC World Congress*, San Francisco, California, July 1996.

20. Penning, K., Zink, P. S., Wei, P., De La Garza, A. P., and Love, M. H., "GLA and Flutter Suppression for a SensorCraft Class Concept Using System Identification," *26th AIAA Applied Aerodynamics Conference*, No. AIAA-2008-7188, Honolulu, Hawaii, Aug. 2008.

Appendix A

Flap Actuator Response

Due to the aeroservoelastic nature of these wind tunnel tests, the frequency responses of the five flap actuators were important. The PID gains on the five control loops were established by examining one actuator loop at a time while tracking a square wave command. Command and position are plotted in near real time on the dSpace1 host system. The procedure for setting the gains is to start with zero integral and derivative gains, and increase the proportional gain until actuator instability, then back off approximately 20 percent. The derivative gain is then adjusted to improve stability. This process is repeated until satisfactory response characteristics are obtained. Integral gain was not found to be useful and was generally set to zero.

Given the fact that GLA testing is quite demanding in terms of the actuator stroke requirements and the number of cycles, the flap actuators' performance was satisfactory. This was especially true for Test 598 where many hours of trimmed flight were successfully demonstrated with the AOS operating. The actuators were, however, the highest maintenance items for Test 598, and three main problems were encountered. The first of these were leaks in the o-rings that seal the actuator shafts. They were a known wear item, and periodic replacement was expected. The other two problems were more troublesome. There was an issue with the end cap o-ring seal where slight variations in the installation procedure and/or lot number variations in the o-rings could lead to part of the o-ring binding against the actuator shaft. This binding would limit actuator bandwidth and linearity, and could be identified by the flap position time trace having a distinctive clipped appearance. Finally, in terms of actuator performance, free play was the biggest problem. Since, the flap position sensor (RVDT) was not attached directly to the actuator shaft, but to the flap, any free play between the actuator shaft and the flap would interfere with the servo control loop.

As part of the start-of-day operations, data was acquired with a 30 s sine-sweep position command being applied to all five flaps. Command and position time histories were acquired, and the actuator transfer functions were estimated using the MATLAB® TFESTIMATE command. Figure A1 shows transfer function estimates for the beginning, the middle, and the end of Test 598. As can be seen, there was some variation in actuator transfer functions throughout the test with flaps TE2 and TE4 having chronic phase issues compared with the other surfaces due the inability to remove the free play.

Cross resonance in the model could also excite the actuator free play in other actuators causing sympathetic limit cycles. In these cases, a reduced proportional gain was needed to maintain stability. By the end of the test, the LE actuator would enter a limit cycle above a dynamic pressure of 60 psf, and it had to be substantially detuned in order to maintain stability as indicated by the large phase lag in figure A1.

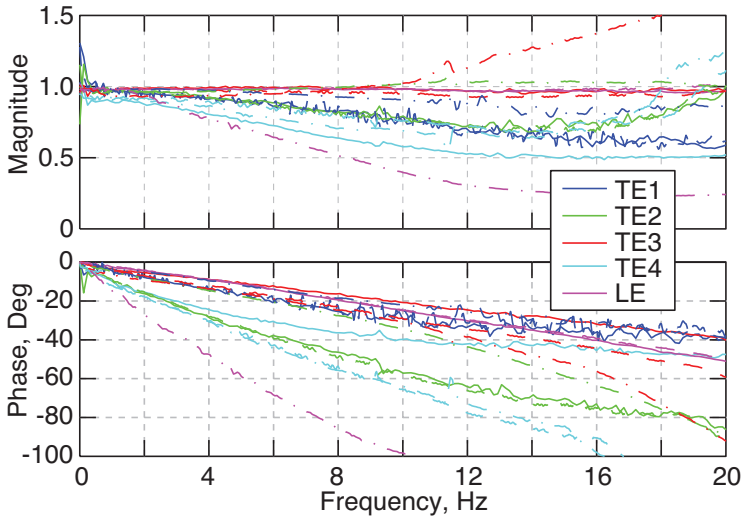

Figure A1. Flap transfer function estimates for beginning (solid), middle (dash), and end (dot dash) of Test 598, points 216, 1600, and 5409.

Appendix B

Snubbing System Performance

This section discusses the performance of the snubbing system as an important consideration for the AEI wind tunnel tests and snubber performance data acquired during Test 593 and Test 598. Figure B1 shows the evolution of the snubber system performance where pitch angle is plotted versus time. These time traces are lined up such that the Snub! command for each was issued at T = 0 s.

The upper part of figure B1 shows the initial testing of the snubber system performance during Test 593. An adjustable flow rate valve was added to the hydraulic line feeding the snubber system to provide some control over the snub rate, and three flow rate settings were considered. Here, with the least restrictive valve setting, the time required to snub the model from the initiation of a Snub! command exceeded 0.5 s, and this setting was used in Test 593. It is interesting to note that these data were acquired when the snubber hydraulics were first installed, and no further timing studies were performed. However, subsequent and frequent operational usage of the snubber system may have resulted in some break-in as the operational snubs indicated a shorter time delay of about 0.3 s. For example, in data from the end of Test 593, plotted in figure 12, there appears to be about 0.3 s of delay between the Snub! command and the pitch angle being clamped.

In preparation for Test 598, the time delay between issuing a Snub! command and the pitch angle being limited and subsequently clamped was a concern. The center plot in figure B1 shows the results of the snubber system timing experiments conducted prior to wing installation. The initial data set (blue) indicated a time delay similar to what was observed in Test 593. As a result, three possible fixes were considered. They were the removal of the flow rate valve, a better method of bleeding the air out, and a diode installed across the solenoid electrical leads. As it turned out, the rotation of the pivot carriage assembly, discussed earlier, ended up being serendipitous as it facilitated bleeding

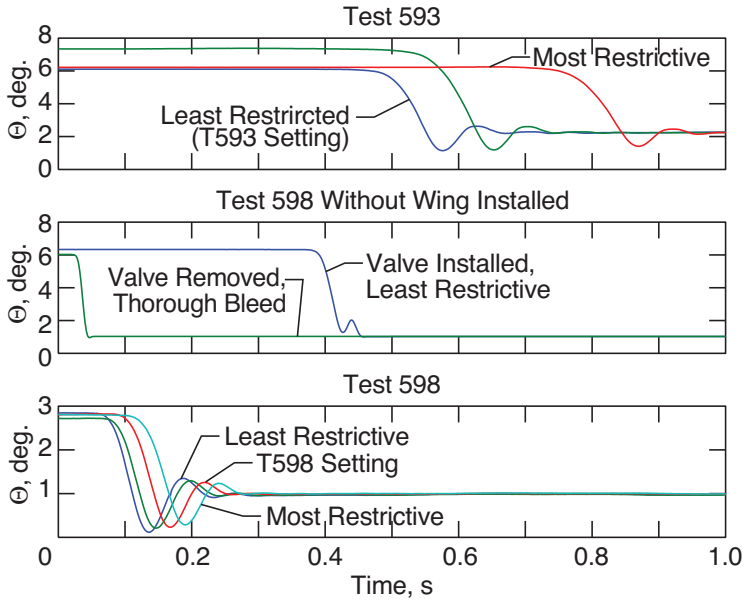

Figure B1. Snubber system time delay experiments, hydraulics at 2000 psi.

the hydraulics. With the actuator in a vertical stroke position, air in the actuator would rise to the top. If the actuator was repeatedly cycled and bled, all the air from the system could be removed. Using this procedure, a satisfactory result was finally obtained as indicated in the center figure.

The lower plot of figure B1 shows snubber timing studies of the system in the final Test 598 configuration. Here, the wing has been installed, the system has been thoroughly bled, and the flow rate valve was used. Several flow rate settings were investigated with the final Test 598 setting identified in the plot where the net time delay was estimated to be 0.15 s.

The reason the flow rate valve was included was that engaging the snubber mechanism could, under some circumstances, induce wing bending loads near limit values. The final flow rate setting was a compromise between snubber speed and induced loads. One known circumstance worth mentioning was air-off snubber engagement where the wing was at maximum Θ. The large difference between the initial and snubbed values of Θ could result in large bending moments. To avoid this problem, the model was electrically snubbed (solenoid valve open) prior to bringing the hydraulic pump on-line. As the initial set point for the pump was 200 psi, the model could be brought to a snubbed state relatively slowly with minimal bending moments. The hydraulic pump would then be brought up to its operational pressure of 2,000 psi.

The snubbing system performed quite well with one minor exception. As the solenoid valve must be energized to unsnub the system, the solenoid coil would heat up during prolonged test sessions. There were several instances during both Test 593 and Test 598 when the snubber mechanism could not be unsnubbed as the valve had apparently stuck in the snubbed position. If the solenoid was left de-energized for approximately 30 minutes, it would start functioning properly again. Installation of a pancake fan to cool the solenoid coil and valve solved the problem during Test 598.

Appendix C

Rail Friction and Lift Augmentation System (LAS)

The consistent behavior and longevity of the LAS and mount system rails were critical to the success of Test 598. These items will be discussed here.

Prior to Test 598, one area of concern was the potential for frequent replacement of the LAS springs. The time involved in clearing the R134a test medium from the TDT along with the time required to change the LAS springs would result in the loss of at least one day of test time. As the model would be flying as close to the vertical center of travel as possible, the center of the LAS springs would receive the most cycles, and data from Test 593 indicated that the vendor-rated life of 13,000 cycles could be reached several times a week. To assess the level of conservatism in the vendors-rated life, a fatigue test of the springs mounted in the LAS assembly was conducted using an Instron machine at NASA Langley Research Center. The springs were pulled out a distance of 12 in to be consistent with the configuration expected with the model flying at tunnel centerline, and the springs were cycled at ± 1 in at 1 Hz. These tests indicated that the springs had a fatigue life of at least 98,000 cycles.

For Test 598, Lockheed Martin introduced the use of load cells to measure the LAS force in the lab, during TDT buildup, and during wind tunnel testing. An additional load cell could be temporarily attached to the wing to measure the force required to lift the wing through its vertical range of motion. Reference 12 describes the extensive rail and LAS friction experiments performed during build-up in the TDT model preparation area. Once the wing, mount, and fairing were assembled in the final test configuration, an abbreviated friction experiment was performed periodically to assess LAS and rail friction. This experiment consisted of acquiring load cell and vertical position data while lifting the wing via the third load cell through its vertical range of motion. Figure C1 shows data acquired at the start of Test 598 and after about 4 weeks of wind tunnel testing. These data indicated a hysteresis loop where force is dependent on the direction of motion. For the purposes of health monitoring, these data were examined for consistency. The data acquired at point 3237 was deemed satisfactory, and the wind tunnel test was continued.

The LAS load cell data was acquired by the DAS and monitored by the test engineers during wind tunnel testing. Figure C2 shows LAS load cell data plotted versus wing vertical position for three different launch and flight sequences. The data from point 3245 indicates a healthy LAS system. Closer examination of these data indicates that during the flight, the LAS friction is no more than ± 1.5 lbs, less than what was measured air-off. The higher vibration environment associated with wind-on operations may improve LAS performance in this regard. The next two data points indicated a weakening and failed forward LAS spring assembly. The LAS system failed twice during Test 598. The first failure was at the point shown here near the middle of the test. To minimize tunnel entries, the model was changed to the light weight configuration when the LAS was repaired. The LAS also failed on the final day of testing.

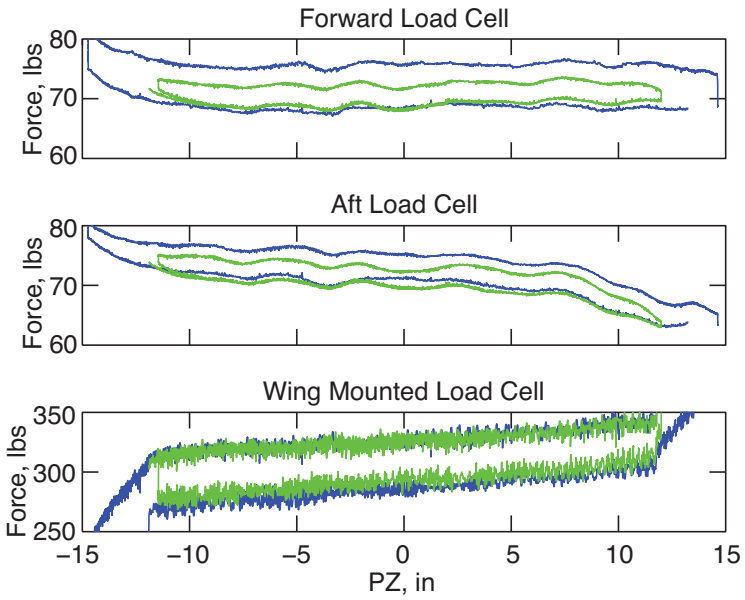

Figure C1. LAS and wing mounted load cell moving average data acquired during wing vertical translation. Test 598, points 212 (blue) and 3237 (green).

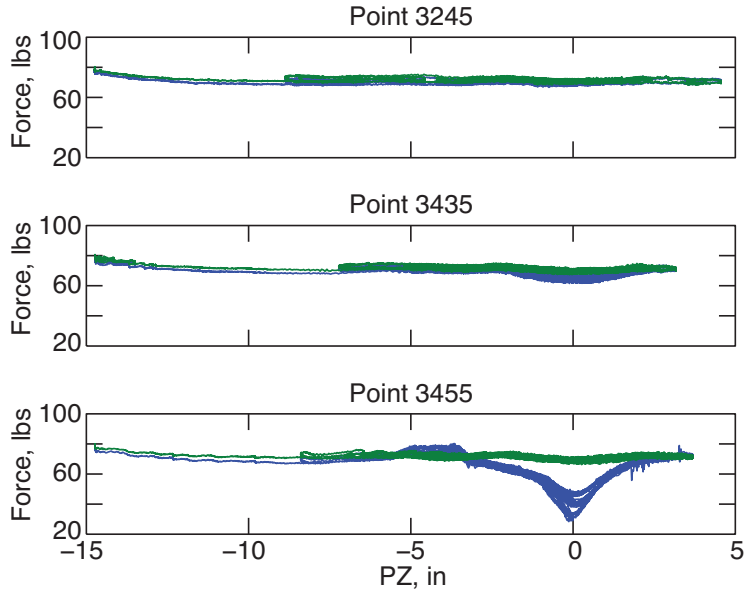

Figure C2. LAS load cell data acquired during three different launch and flight sequences. Test 598, points 3245, 3435, and 3455. (Forward load cell data is blue and the aft load cell data is green).

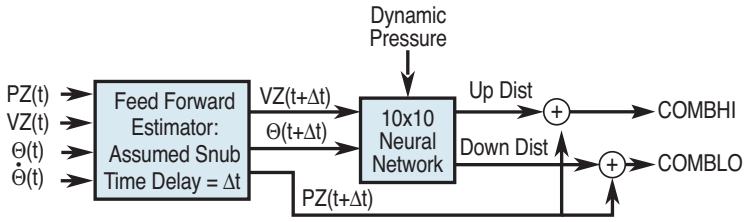

Figure D1. Lockheed Martin combined parameter block diagram.

Appendix D

Development of LM Combined Parameters

A significant analysis effort was undertaken by Lockheed Martin Aeronautics to determine additional WatchDog parameters so that a Snub! command would be issued in time to snub the model and subsequently control plunge displacement using the emergency controller before the pivot carriage hit the shocks. These combined parameters needed to take into account the time delay in physically snubbing the model and the vertical travel needed by the emergency controller to obtain a zero sink rate. This appendix will describe how the LM combined parameters were developed, verified, and implemented.

A simulation model of the wing, mount system, and control systems was developed in MATLAB® Simulink. The wing, including the mass of the pivot carriage assembly, was modeled using a series of state-space models for various combinations of Mach number and dynamic pressure with two-dimensional interpolation used to generate the ASE model for at a given flight condition. The ASE model contained inputs for five control surface position commands and a vertical gust velocity input. The physical constraints and forces associated with the rest of the mount system were imposed on the wing root using six force/moment inputs (x, y, z, roll, pitch, yaw). The effects of mount flexibility were modeled using these force terms. In the case of the vertical force, terms for friction as a function of bending moment, the LAS, the shocks, and the hard stop were included. The pitch moment force included terms for the pitch shock absorbers, hard stop, and the pitch clamp actuator. The outputs of the ASE model were the 23 aircraft sensors.

A series of simulations were run to determine the relationship between the initial condition of the model and vertical travel needed to obtain a zero sink rate. The simulation started with an initial vertical rate, pitch angle, pitch rate, and dynamic pressure for both the heavy and light model configurations. The initial conditions for all other parameters were assumed to be zero. The time delay between Snub! command and a pitch restoring force being applied to the wing root was also assumed to be zero. The simulation studies indicated that if the model was not snubbed at the time of pivot carriage to shock contact, large pitch excursions and wing bending moments would result. Thus, wing bending moments were within allowable limits as long as the model was snubbed prior to vertical shock contact. These simulation data were then used to construct a new WatchDog parameter. The parameter was generated by determining the relationship between vertical velocity, pitch angle, and dynamic pressure and the vertical distances up or down needed to stop the model once the snubber had been engaged. This mathematical relationship was represented by a 10 by 10 neural network.

In order to account for any time delay between the Snub! command and pitch snub mechanism physical engagement, some parameters were extrapolated into the future. A

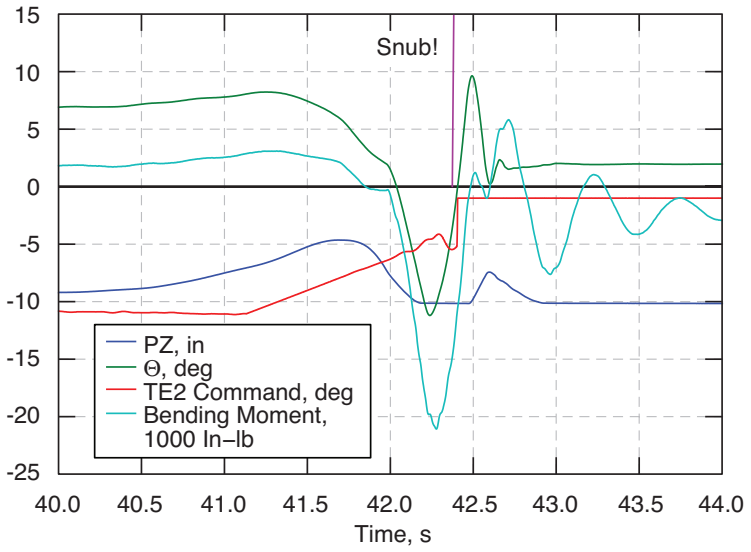

Figure D2. Hard landing case plot of vertical position, pitch angle, TE2 command, and wing root bending moment with Snub! command indicated. Test 593, point 1252. The bending moment is measured from strain gauge SBI1 shown in figure 8 corrected for outboard wing weight.

simple feed forward estimation routine using an assumed snubber time delay was applied to vertical position, vertical rate, pitch angle, and pitch rate. The forward estimator and neural network were combined in series in the WatchDog system as shown in figure D1 to provide a real-time estimate of the vertical position, up or down, where the model would be brought under control. These values were monitored by the WatchDog system, and as with the other monitored signals, the WatchDog would issue a Snub! command when thresholds were exceeded.

To assess snubber time delay requirements, five hard landing cases from Test 593 were examined. For one of these data points, figure D2 plots the time histories of vertical position, pitch angle, Snub! command, TE2 command, and wing root bending moment. The figure shows that the model starts to climb then falls back, lands hard, and bounces. Pitch angle and bending moment decrease rapidly after contacting the shocks just before T = 42 s where slope discontinuities are observed in the vertical position, pitch angle, and bending moment time histories. These data are consistent with the simulation results indicating the need to have the model clamped in pitch prior to shock contact to minimize subsequent pitch angle excursions and high wing bending moments.

For the five hard landing cases, the performance of the WatchDog system monitoring only the original measured parameters was compared with the WatchDog system configured to monitor the LM combined parameters using two different assumed snubber time delays of 0.1 and 0.25 s. Figure D3 shows one of these hard landing cases where the model vertical position and pitch angle are plotted along with the Snub! command associated with the three WatchDog configurations. Shock contact is indicated by the red line. For this data point, the original WatchDog system would have snubbed the model as it was descending through a −10 in/s velocity threshold. The combined parameter cases caught the model earlier, as shown. The figure of merit for these cases is the time difference between shock contact and when the command was issued. If the actual, physical snubber time delay is less than the required time delay, then a given WatchDog parameter would have been successful

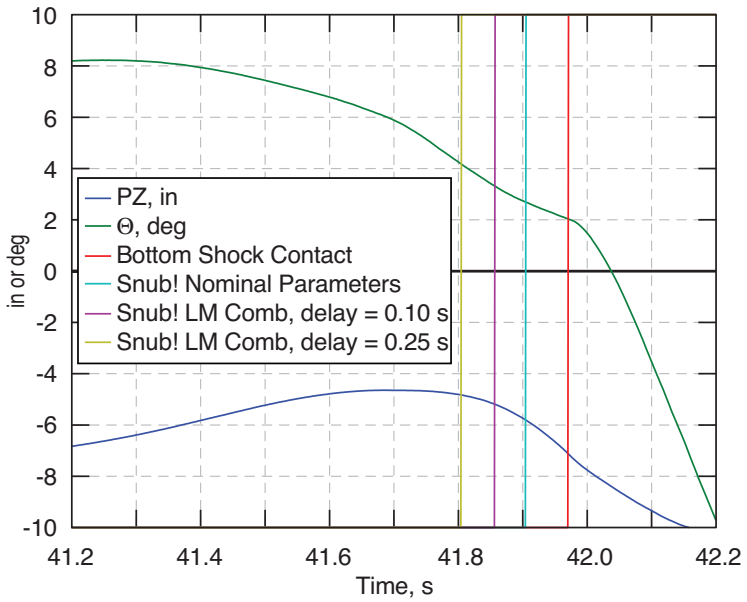

Figure D3. Hard landing case comparing nominal WatchDog Snub! command with the Snub! command generated by the LM combined parameters where two values of assumed time delay were used in the feed forward estimator. Test 593, point 1252.

Table D1. WatchDog system performance assessed using five hard landing cases from Test 593.

Assumed Snub Time Delay, s	Required Time Delay, s (pt. 1252)	WD Performance In-Time	WD Performance False Alarm
	0.065	2/5	1/5
0.10	0.113	5/5	0/5
0.25	0.165	2/5	1/5

in avoiding model and shock contact and high loads.

Table D1 shows the required time delay for the data point in figure D3 along with a summary of the performance of the WatchDog system for all five Test 593 cases examined. A false alarm is defined as a case where a Snub! command is issued, but the bending load limits were not subsequently exceeded in the data set. The combined parameter with an assumed 0.1 s snubber time delay was able to snub the model before contacting the shock in all five cases with no false alarms. As previously discussed, the physical snubber system was ultimately configured to provide a delay of 0.15 s, and this value was used in feed forward estimator to compute the LM combined parameters during Test 598. The WatchDog performance in Test 598 was satisfactory.

REPORT DOCUMENTATION PAGE

Form Approved
OMB No. 0704-0188

The public reporting burden for this collection of information is estimated to average 1 hour per response, including the time for reviewing instructions, searching existing data sources, gathering and maintaining the data needed, and completing and reviewing the collection of information. Send comments regarding this burden estimate or any other aspect of this collection of information, including suggestions for reducing this burden, to Department of Defense, Washington Headquarters Services, Directorate for Information Operations and Reports (0704-0188), 1215 Jefferson Davis Highway, Suite 1204, Arlington, VA 22202-4302. Respondents should be aware that notwithstanding any other provision of law, no person shall be subject to any penalty for failing to comply with a collection of information if it does not display a currently valid OMB control number.
PLEASE DO NOT RETURN YOUR FORM TO THE ABOVE ADDRESS.

1. REPORT DATE *(DD-MM-YYYY)*	2. REPORT TYPE	3. DATES COVERED *(From - To)*
01- 10 - 2013	Technical Publication	

4. TITLE AND SUBTITLE

Aeroservoelastic Testing of Free Flying Wind Tunnel Models Part 1: A Sidewall Supported Semispan Model Tested for Gust Load Alleviation and Flutter Suppression

5a. CONTRACT NUMBER

5b. GRANT NUMBER

5c. PROGRAM ELEMENT NUMBER

6. AUTHOR(S)

Scott, Robert C.; Vetter, Travis K.; Penning, Kevin B.; Coulson, David A.; Heeg, Jennifer

5d. PROJECT NUMBER

5e. TASK NUMBER

5f. WORK UNIT NUMBER

473452.02.07.04.02.01

7. PERFORMING ORGANIZATION NAME(S) AND ADDRESS(ES)

NASA Langley Research Center
Hampton, VA 23681-2199

8. PERFORMING ORGANIZATION REPORT NUMBER

L-20308

9. SPONSORING/MONITORING AGENCY NAME(S) AND ADDRESS(ES)

National Aeronautics and Space Administration
Washington, DC 20546-0001

10. SPONSOR/MONITOR'S ACRONYM(S)

NASA

11. SPONSOR/MONITOR'S REPORT NUMBER(S)

NASA/TP-2013-218051

12. DISTRIBUTION/AVAILABILITY STATEMENT

Unclassified - Unlimited
Subject Category 01
Availability: NASA CASI (443) 757-5802

13. SUPPLEMENTARY NOTES

14. ABSTRACT

This is part 1 of a two part document. Part 2 is titled: "Aeroservoelastic Testing of Free Flying Wind Tunnel Models, Part 2: A Centerline Supported Fullspan Model Tested for Gust Load Alleviation." A team comprised of the Air Force Research Laboratory (AFRL), Northrop Grumman, Lockheed Martin, and the NASA Langley Research Center conducted three aeroservoelastic wind tunnel tests in the Transonic Dynamics Tunnel to demonstrate active control technologies relevant to large, flexible vehicles. In the first of these three tests, a semispan, aeroelastically scaled, wind tunnel model of a flying wing SensorCraft vehicle was mounted to a force balance to demonstrate gust load alleviation. In the second and third tests, the same wing was mated to a new, multi-degree of freedom, sidewall mount. This mount allowed the half-span model to translate vertically and pitch at the wing root, allowing better simulation of the full span vehicle's rigid body modes. Gust load alleviation (GLA) and Body freedom flutter (BFF) suppression were successfully demonstrated. The rigid body degrees-of-freedom required that the model be flown in the wind tunnel using an active control system. This risky mode of testing necessitated that a model arrestment system be integrated into the new mount. The safe and successful completion of these free flying tests required the development and integration of custom hardware and software. This paper describes the many systems, software, and procedures that were developed as part of this effort.

15. SUBJECT TERMS

Active control; Aeroservoelasticity; Body freedom flutter; Flutter suppression; Gust load alleviation; Wind tunnel tests

16. SECURITY CLASSIFICATION OF:			17. LIMITATION OF ABSTRACT	18. NUMBER OF PAGES	19a. NAME OF RESPONSIBLE PERSON
a. REPORT	b. ABSTRACT	c. THIS PAGE			STI Help Desk (email: help@sti.nasa.gov)
					19b. TELEPHONE NUMBER *(Include area code)*
U	U	U	UU	50	(443) 757-5802